Intron retention as a new marker of the pre-disease state and its recovery to the normal state by a traditional Japanese multi-herbal medicine

Running title: Recovery of alternative splicing from the senescence to healthy type by an herbal medicine

Norihiro Okada[a#], Kenshiro Oshima[a$], Yuki Iwasaki[a$], Akiko Maruko[a], Erica Iioka[a], Trieu-Duc Vu[a], Naoki Fujitsuka[b], Akinori Nishi[b], Aiko Sugiyama[b], Mitsue Nishiyama[b], Atsushi Kaneko[b], Masahiro Yamamoto[b] and Susumu Nishimura[ac]

[a] Foundation for Advancement of International Science, 3-24-16 Kasuga, Tsukuba, Ibaraki 305-0821 Japan,
[b] Tsumura Kampo Research Laboratories, Tsumura & CO., 3586 Yoshiwara, Ami-machi, Ibaraki 300-1192 Japan,
[c] Laboratory Animal Resource Center, University of Tsukuba, 1-1-1 Tennodai, Tsukuba, Ibaraki 305-8575 Japan

[$] These two authors contributed equally to this work.
[#] To whom correspondence should be addressed.
nokada@fais.or.jp

Key words: RNA-seq, Kampo, senescence, alternative splicing, intron retention

Abbreviations: Cten: cell type enrichment analysis; DEG: differentially expressed genes; FC: fold change; GO: Gene Ontology; JTT: Juzen-taiho-to; IGV: Integrative Genomics Viewer; IR: intron retention; IJC: inclusion junction count; Kampo: Japanese multi-herbal medicines; KL: klotho mice; SJC: skipping junction count; RNA-seq: RNA sequencing; pre-mRNA: precursor mRNA; SE: skipped exon; TF: transcription factor; WT: wild type; 3-HBA: 3-hydroxybutyric acid

Abstract

Intron retention (IR) is an important regulatory mechanism that affects gene expression and protein functions. Using klotho mice as a model, we proposed that retained introns are an excellent marker for the pre-disease state. Surprisingly, among widespread retained introns that accumulated during aging in the liver, a subset was recovered to the normal state by a Japanese traditional herbal medicine. IR-recovered genes fell into two categories: (1) those involved in the spliceosome and (2) those involved in liver-specific metabolism. By integrating data for splicing patterns, transcriptomes, and metabolomes, we hypothesize that this medicine-related IR recovery under the pre-disease state reflects the actual recovery of liver-specific function to the healthy state. Accordingly, the study provides proof-of-concept evidence related to the ancient Chinese statement proposing the medicine's usefulness for treating the pre-disease state. This approach lays out a method for elucidating unknown molecular mechanisms of an herbal medicine with multiple ingredients. (149 words)

Introduction

The vast majority of precursor mRNAs (pre-mRNAs) in mammalian cells consists of exons separated by introns. Introns are normally removed by a mechanism called splicing, which leaves the joined exons that form the mature mRNA (Padgett et al., 1986, Patel and Steitz, 2003). The process of removing an intron from pre-mRNA is highly dynamic, during which a complex rearrangement of protein-protein, RNA-RNA, and RNA-protein interactions takes place in the spliceosome (Mayeda et al., 1994). Because of such complexity, the process is highly vulnerable to external stimuli (Stegeman and Weake, 2017). Dysregulation of RNA splicing has been identified as a causative defect in several diseases, especially in cancer (Dvinge et al., 2016).

It has recently become widely recognized among molecular biologists that aging reflects the gradual deterioration of the molecular components of the cell, the concerted functioning of which are vital for cell viability and proliferation (Lopez-Otin et al., 2013). In this sense, aging is regarded as a kind of disease, the extent of which varies among individuals. The complexity of alternative splicing of pre-mRNAs makes this process vulnerable even to aging, as suggested by many instances in which aging is accompanied by a change in the expression level of spliceosomal proteins or by a change in their splicing patterns (Zane et al., 2014). For example, levels of SF3B1 and

SRSF family proteins can be affected by changes in alternative splicing during aging (Deschenes and Chabot, 2017). As these changes in turn may alter the alternative splicing of numerous transcripts, a change in the expression of spliceosomal and associated proteins is primarily important.

Intron retention (IR) is one of the forms of alternative splicing and is considered to be harmful to the organism by (1) slowing down splicing kinetics to delay the onset of gene expression (Braunschweig et al., 2014), (2) increasing pre-mRNA degradation in the nucleus by nuclear exosomes (Niemela et al., 2014), and (3) increasing (pre-)mRNA degradation in the cytoplasm by nonsense-mediated decay (Lejeune and Maquat, 2005). IR accumulation has even been proposed as a post-transcriptional signature of aging (Adusumalli et al., 2019). Analyses of the transcriptome from mouse, human brain, and Drosophila head have shown a global increase in the level of IR during aging, indicating that this process may be evolutionarily conserved (Adusumalli et al., 2019).

In the present study, we used the klotho mouse, which is a model for senescence and exhibits a syndrome resembling human aging that includes a reduced life span, decreased activity, infertility, osteoporosis, atherosclerosis, atrophy of the skin, and emphysema (Kuro-o et al., 1997). This phenotype is caused by the disruption of a single gene, klotho (*Kl*). In a normal mouse, the klotho protein and FGF23 function as a receptor in the kidney to exert a diuretic action on phosphorus (Razzaque, 2009). In a klotho mouse, however, the blood level of phosphorus is very high because of a deficiency in the klotho protein, which leads to rapid senescence in this mouse.

Japanese multi-herbal medicines (Kampo) originated in ancient China and are widely used in Japan for various disorders. In contrast to chemically synthesized Western drugs, whose effects on humans are carefully evaluated during various stages of testing and whose mechanisms of actions are generally rigorously evaluated, it has been difficult to identify the molecular substances in the Kampo that are responsible for their potency and to analyze the mechanisms by which they exert their effects. It has long been said that thousands of chemical compounds in Kampo work together, sometimes synergistically, and that their side-effects, if any, are relatively minor, although their mechanism of action remains a total mystery (Zhou et al., 2016).

Juzen-taiho-to (JTT), being composed of 10 crude drugs as one of the formulations approved as a medicine in Japan, was first described in a drug textbook in the Song Dynasty (AD 1151) in China and was introduced in Japan during the Kamakura period (Saiki, 2000) (AD 1185–1333). It has been traditionally administered to patients with deficiency syndrome, consisting of disturbances and imbalances in the homeostatic condition of the body (Onishi et al., 1998). More specifically, it is prescribed for

patients with fatigue, anemia, night sweats, anorexia, or circulatory problems. JTT has stimulatory effects on the immune response including enhancement of phagocytosis, cytokine induction, induction of mitogenic activity of spleen cells, and activation of macrophage and natural killer cells (Matsumoto et al., 2000). JTT can also prolong life when combined with the surgical excision of tumors and has a protective effect against the deleterious effects of chemotherapy drugs (Wang et al., 2018).

Knowing that aging can lead to an increase in retained introns, we used klotho mice that had not yet undergone extensive aging and examined the effects of JTT on IR patterns in genes expressed in their organs by using an RNA sequencing (RNA-seq) analysis (Vu et al., 2019). We discovered that IR occurred even during this earlier stage in the aging process when no change in protein level and no pathological changes in the organs were observed and can thus be used as a new marker of the pre-disease state. Detection of the pre-disease state is important for human health, because the state can be reversible when it is appropriately treated. Here we provide definitive evidence that JTT can specifically decrease the retained introns of genes for liver metabolic functions among those that show an increase during the process of aging. With the support of both transcriptome data related to differentially expressed genes (DEGs) and changes in the metabolome, we suggest that JTT has a beneficial effect on metabolism in the liver at an earlier stage of aging. We thus propose that the decrease in liver IR at this earlier stage of aging by JTT is an indication of the effective actions of this herbal medicine at the time corresponding to the pre-disease stage.

Results

Looking for a marker of the pre-disease state in klotho mice at 7 weeks of age

We used klotho mice, a model mouse for aging, for our experiment to look for a new marker for the pre-disease state as well as a possible effect of a Japanese herbal medicine on this state. Because aging is currently regarded as a kind of disease (see Introduction), the pre-aging state can be regarded as a pre-disease state. We have chosen the time of 7 weeks after birth for the date of sampling (Fig. 1AB), which is less than half of the half-life of these mice (14.7 weeks; Fig. 1B). We expected that markers, if any, isolated from these mice at 7 weeks would represent the pre-disease state. We also designed our experiments to examine the effect of JTT on the improvement of the pre-disease state (Fig. 1A). We designated klotho mice as KL and wild-type mice as WT,

each of which was fed with (+) or without (–) 0.5% JTT from 3.5 weeks of age until the mice were 7 weeks old.

First, to examine the extent of aging of liver tissue in klotho mice, we looked for histological changes at 7 weeks of age relative to liver tissue in WT mice. Fig. 1C shows that there was no such alteration, indicating that the liver did not exhibit a senescent phenotype at this age. Second, we chose several proteins and examined their protein level by performing western blotting analysis (Fig. 1D). The representative proteins are DDX5, SRSF6, and NXF1, all of which are splicing-related genes, and PPARD and SIRT7, both of which are involved in metabolic pathways of the liver. NDUFS2 is the core subunit of the mitochondrial Complex1, and LXRβ is encoded by *Nr1h2* and regulates macrophage function. GAPDH was used as the loading control. Furthermore, we checked the expression of RGN/SMP30, a marker of senescence whose expression decreases with aging (Maruyama et al., 2010) (Fig. 1E). There was no observable difference in the expression of these proteins between KL– and WT– (Fig. 1DE), and thus we can conclude that the klotho mouse liver at 7 weeks of age does not show clear signs of aging.

Metabolome analysis shows that klotho mice at 7 weeks of age express starvation-like characteristics

To look for possible internal changes in the liver that could describe the pre-disease state in this earlier stage of aging, we investigated 110 metabolites of the liver using CE-TOFMS (CE: capillary electrophoresis, TOFMS: time-of-flight mass spectrometry), and compared metabolite levels between KL– and WT–, the comparison of which is a measure of senescence. Among 12 metabolites that showed such differences, the data for 7 metabolites ($P < 0.05$) are shown in Fig. 2. Remarkably, 3-hydroxybutyric acid (3-HBA) was significantly increased in KL– (Fig. 2A), to a level 2.5 times higher than that in WT–. 3-HBA is synthesized in the liver from fatty acid as one of the ketone bodies under conditions of starvation and can be used as an energy source when blood glucose is low (Fukao et al., 2014). Consistent with this, certain intermediate metabolites of glycolysis, namely glucose 1-phosphate, fructose 1,6-diphosphate, dihydroxyacetone phosphate, lactic acid, CoA divalent, and alanine in KL– were significantly decreased as compared with their levels in WT– (Fig. 2B). These data suggest that klotho mice are undergoing a fasting state, in spite of the presence of ample food, during which the synthesis of 3-HBA is activated. Accordingly, an increase in 3-HBA and a reduction in glycolysis in KL– might be representative of senescence in klotho mice.

DEG analysis shows the alteration of gene expression during aging

Knowing that the liver of klotho mice is under the starvation-like condition, we performed RNA-seq analysis to look for a possible alteration of the gene expression level in the liver during the pre-disease state. From liver collected from KL+, KL–, WT+ and WT–, we isolated the mRNAs and then sequenced them. Multi-dimensional scaling confirmed the consistency of each dataset (Fig. S1A). In addition, transcriptomes from individual organs from KL+ and KL– indicated that JTT induced extensive transcriptome changes (Fig. S1B).

We then extracted a down-regulated gene set and an up-regulated gene set in KL– from the comparison of KL– and WT– (1228 genes and 1352 genes, respectively; Fig. 3A). The former represents genes whose expression decreased in the liver probably due to aging-related deterioration, and the latter represents genes whose expression increased possibly reflecting an adaptive response to aging. To characterize enriched cell types in these genes, we performed a cell type enrichment (Cten) analysis (Shoemaker et al., 2012) by using the software provided by these authors, in which, for each cell type, a transcript was defined as a highly expressed cell-specific gene in that cell if it had an expression value at least 15× greater than its median expression value across all cells examined. The software can accurately identify the appropriate cell type in a highly heterogeneous environment and provides insight into the suggested level of enrichment to minimize the number of false discoveries. Fig. 3C shows that liver-specific genes were especially enriched among the genes whose expression decreased during aging, suggesting that liver function was reduced during aging. In contrast, a variety of non-liver-specific cell types were enriched among those genes whose expression increased during aging (Fig. 3D). It should be noted that several macrophage-related cells were enriched in these increased genes, consistent with the generally believed notion that the aging process activates innate immunity in spite of its severe deterioration of adaptive immunity (Solana et al., 2006).

DEG analysis shows the improvement in liver function as a result of JTT administration

To examine the influence of administration of JTT on the gene expression level in the livers of klotho mice, we extracted the set of genes that were up-regulated and down-regulated in KL+ after administration of JTT from the comparison of KL+ and KL–

(532 genes and 412 genes, respectively; Fig. 3B). Cten analysis of the up-regulated genes demonstrated that liver-specific genes were highly enriched (Fig. 3E), whereas that of down-regulated did not exhibit any enrich https://orcid.org/0000-0002-3655-8060
ent. A comparison of the up-regulated gene set from the comparison of KL+ and KL– (532 genes) and the down-regulated gene set in KL– from the comparison of KL– and WT– (1228 genes) resulted in 213 DEGs, each of which exhibits the clear recovery pattern from the decreased level of KL– to the level of WT– in the KL+ (Fig. 3F). Fig. 3G shows a boxplot summarizing the expression of 213 genes. Each data point was normalized to the average expression level of each gene, and all the data were summed. By using these genes, we performed a Cten analysis as shown in Fig. 3H and showed that liver-specific functions are highly enriched in the 213 genes. We then extracted GO terms enriched for these genes. Fig. 3I shows that genes related to liver-specific functions, including metabolic process, flavonoid biosynthetic process, flavonoid glucuronidation, and lipid metabolic process, were enriched, suggesting that the liver functions were recovered by administration of JTT.

IR and its recovery after administration of JTT is most prominent in the liver

Knowing that klotho mice at 7 weeks of age represent a starvation-like state and that their liver-specific functions at that time might be reduced due to the decreased expression of liver-specific genes, we looked for possible changes in alternative splicing at this age because it is known that several stresses can change alternative splicing patterns (Boutz et al., 2015, Ninomiya et al., 2011, Shalgi et al., 2014; see later discussion). We performed RNA-seq analysis in additional three organs, namely, blood, kidney and heart for comparison.

To identify what type of alternative splicing is most prominent in the four organs examined here, we first analyzed five types of alternative splicing, namely alternative 5' splice site, alternative 3' splice site, skipped exon (SE), IR, and mutually exclusive exons, between KL+ and KL– by using rMATS (Table 1-1). SE and IR were the most prominent types of alternative splicing among the four organs. Noticeably, a change in the frequency of IR in the liver was the most prominent effect followed by that in the blood (Table 1-1).

We then calculated the difference in the frequency of IR in comparisons among KL+, KL–, WT+, and WT– with the criteria of $P < 0.01$ (Table 1-2). We first noticed a difference in the frequency of retained introns for the comparison between KL+ and

WT– was noted for only 59 loci, whereas that for KL– and WT– was noted for 212 loci. The comparison between KL+ and WT– is a measure of the effect of JTT over senescence, whereas the comparison between KL– and WT– measures the effect of the senescence level in terms of the extent of retained introns accumulated during aging in klotho mice. The above data suggest that the administration of JTT shifted the AS pattern in klotho mice to be more similar to that of WT mice.

The 142 IR loci (Table 1-1 & -2) that were differentially affected between KL+ and KL– in the liver included those genes for which the frequency of IR was decreased with JTT in KL+ (132 loci; designated as "DecIR" type) and those genes for which the frequency of IR was increased with JTT in KL+ (10 loci; designated as "IncIR" type) (Fig. 4A). Likewise, the comparison between KL+ and KL– for the other three organs showed a number of differential IR loci that could be divided into these two types. The liver and blood exhibited higher values in the DecIR type as compared with the IncIR type, whereas the other two organs, kidney and heart, had comparable values for DecIR and IncIR (Fig. 4A). From these data, we designated liver and blood as two target organs for JTT. Since we showed that the liver-specific function was recovered by administration of JTT (see above), we focused in particular on the analyses of genes that underwent a decrease in IR in the liver in response to JTT.

Analysis of IR-recovered genes in the liver

To demonstrate our strategy for evaluating the extent of IR, we first show an example based on the data for *Anxa11* expression in the liver (Fig. 4C). *Anxa11* plays an important role in cell division, Ca^{2+} signaling, vesicle trafficking, and apoptosis (Han et al., 2017). Sequenced *Anxa11* transcripts showed extensive accumulation of a retained intron in KL–, whereas this intron was retained to a lesser extent for KL+ and WT– (Fig. 4Ci).

Then, to analyze IR of *Anxa11* mathematically, we calculated the read counts of skipping junctions (SJCs) and those of inclusion junctions (IJCs) for KL+, KL–, and WT– (Fig. 4Cii) according to the strategy illustrated by rMATS (Fig. 4B). For KL+, we then took the base-2 logarithm of the SJC/IJC ratio, which gives the fold change (hereafter designated as FC) between the SJC and IJC at the intron junction (the thick black bars in Fig. 4Ci). The same process was carried out for KL– and WT–, and the FC values for KL+, KL–, and WT– were compared. The lower FC value for KL– was recovered in KL+ to the same level as that of WT– (Fig. 4Ciii). The V shape of this bar

plot indicated a recovery from the senescence-type IR to the healthy-type IR after JTT administration (see below).

As was described above, we first obtained the DecIR type (132 loci, 124 genes) in klotho mice caused by JTT administration by comparing KL+ vs KL–. This simply represents the recovery of retained introns in KL+. Then, we obtained the IncIR type (190 loci, 180 genes) in klotho mice by comparing KL– vs WT–. This represents a measure of the senescence-related changes in retained introns. Accordingly, the comparison between these two types allowed us to highlight the effect of JTT at 7 weeks of age as shown in a Venn diagram (Fig. 5A). The overlapping 70 loci (67 genes) represent the “complete recovery” loci, which are defined as those with significant differences between KL+ and KL– and between KL– and WT–, but with FC values for KL+ and WT– that were similar. The non-overlapping 62 (61 genes) and 120 loci (115 genes) represent "partial recovery" and "no recovery" loci, respectively. Fig. 5B shows a heatmap of the 70 “complete recovery” loci, each of which represents a clear recovery pattern. Fig. 5C is a boxplot of the FC values of KL+, KL–, and WT– for these 70 loci, which shows the typical V-shaped pattern of recovery. Fig. 5D & E show boxplots of the “partial recovery” loci and the “no recovery” loci, respectively. The former represents loci with a significant difference between KL+ and KL– and without a significant difference between KL– and WT–. The latter represents loci with a significant difference between KL– and WT– and without a significant difference between KL+ and KL–.

Characteristics of loci with retained introns in the liver

We next characterized introns among the 70 “complete recovery” loci, the 120 “no recovery” loci and all other genes (~250,000 loci) expressed in the liver. The average length of introns from the “complete recovery” and “no recovery” loci was significantly shorter than that of all other introns (Fig. 6A). There was, however, no significant difference in intron length between the “complete recovery” and “no recovery” loci, suggesting that the “complete recovery” loci were not selectively discriminated from the “no recovery” loci during the recovery process associated with JTT administration. The GC content of introns associated with the “complete recovery” and “no recovery” groups was significantly higher than that of all other liver-related introns (Fig. 6B). Also, there was no significant difference between “complete recovery” and “no recovery” introns in this respect, suggesting that GC content was not linked to recovery status among IR loci. Then, we examined the strength of 5' and 3' splice sites by

calculating scores for these splice sites using the software MaxEntScan. The 5' splice sites of introns of the "complete recovery" and "no recovery" loci were slightly but significantly weaker than those of all other liver-related introns (Fig. 6C), but we found no such differences at the 3' splice sites (Fig. 6D). These characteristics of introns at IR loci were observed in the three additional organs (see below and Fig. S2A–D) and are consistent with previous data (Braunschweig et al., 2014). Thus, loci with shorter intron lengths, a higher GC content, and a weaker splicing score at the 5' site have a tendency to have retained introns, but these are not characteristics that make retained introns more likely to undergo recovery in the presence of JTT in the klotho mice. We also confirmed the susceptibility of introns to IR in genes in terms of their shorter intron length, higher GC content, and weaker intron score at the 5' splice site in the other three organs (Fig. S2A–D) as was shown in the case of liver (Fig. 6).

Next, we searched for possible enrichment of binding sites for RNA-binding proteins in the introns, as these are known to influence splice site selection and are required for splicing (Padgett et al., 1986,Patel and Steitz, 2003). Binding sites for five RNA-binding proteins were especially enriched in introns among the 70 "complete recovery" loci but not among the 120 "no recovery" loci (Fig. 6E). This suggests that genes expressed in the liver were more likely to recover from IR after JTT treatment if they had these RNA-binding sites. Likewise, we examined the tendency for enrichment for transcription factors (TFs) that bind to promoter regions in liver and in blood. Binding sites for four TFs (Hoxa10, Hoxd12, Hoxd10, and Hoxd13) were especially enriched in "complete recovery" genes in comparison with "no recovery genes" in liver (Fig. 6F).

Validation of IR-recovered genes in the liver by using RT-PCR

Eleven genes were chosen for Integrative Genomics Viewer (IGV) mapping and RT-PCR, which confirmed the recovery of IR upon JTT administration (Fig. 7, Fig. S3). These genes are involved in RNA splicing (*Ddx5, Srsf5*) and typical liver functions such as glucose and fatty acid metabolic pathways (*Sirt7*, *Acadm*, *Decr2*, *Gnmt*), lipid metabolic processes (*Acadm*), heme biosynthesis and bile acid production (*Cyp27a1*, *Hsd3b7*), and oxidation-reduction processes (*Acadm*, *Cyp27a1*, *Hsd3b7*).

Biological function of IR-recovered genes in the liver

Possible effects of JTT on the selection of liver retained intron loci for recovery during aging were analyzed (Fig. 8). The results obtained from the Gene Ontology (GO) analysis using Biological Process terms in Fig. 8A & B suggest two conclusions. First, in the comparison between DecIR type (132 loci, 124 genes) of KL+ vs KL– and IncIR type (190 loci, 180 genes) of KL– vs WT–, genes involved in RNA splicing and mRNA processing are susceptible to IR during the aging process, and these retained introns tend to be recovered by JTT (i.e., the red and blue bars are comparable; Fig. 8A). The tendency of genes involved in these processes to be susceptible to IR during aging is consistent with a previous study (Zane et al., 2014). These splicing-related genes can control the expression of downstream genes through the regulation of their alternative splicing. We defined 250 genes as potential splicing-related genes to highlight their importance in the regulation of alternative splicing (see Methods for the definition of splicing-related genes). They included almost all the spliceosomal proteins and spliceosome regulatory proteins. Among 368 gene loci that exhibited a difference in alternative splicing for the comparison of KL+ and KL– in the liver (Table 1-2), 19 genes (data not shown) were detected among the list of 250 potential splicing-related genes. Among these 19 genes, 9 potential splicing-related genes in the liver were subjected to IR, all of which exhibited the recovery pattern in terms of the comparison in the FC among KL+, KL–, and WT– (Table 2). The patterns of recovery of the seven potential splicing-related genes in liver associated with JTT administration together with their FC values are shown in Fig. 7, Fig. 8D(i–iii), and Fig. S5B. Accordingly, JTT appears to work in the direction of recovery, especially for potential splicing-related genes.

Second, in addition to the recovery of IR for genes related to RNA splicing and RNA processing, IR recovery was not evenly distributed among genes that accumulated retained introns during aging but instead occurred selectively among liver-specific genes. This conclusion was more obvious when loci of “complete recovery” (70 loci) and “no recovery” (120 loci) were compared (Fig. 8B). The GO terms metabolic process, oxidation-reduction process, carbohydrate metabolic process, and regulation of gluconeogenesis, which represent major functions of the liver, were enriched among genes that underwent “complete recovery” (i.e., red bars), whereas genes in the “no recovery” group are associated with more general functions such as translation, protein transport, and apoptosis (i.e., blue bars). These data suggest that, among genes susceptible to IR during aging, the liver-specific genes selectively underwent a shift in retained introns from the senescent state to the normal state after administration of JTT.

To further confirm that the recovery of retained introns by administration of JTT occurred in liver-specific genes, Cten analysis was performed as shown in Fig. 8C. Genes with "complete recovery" were significantly enriched among liver-specific genes ($-\log_{10} P = 6.040$), confirming that the IR recovery from aging specifically occurred in liver-specific genes.

Biological function of IR-recovered genes in the blood

To examine the characteristics of recovered genes among the other three organs, GO analysis was performed for these organs, but only in the case of blood was the significant enrichment of pathways with $P < 0.05$ observed (data not shown). GO analysis for genes expressed in the blood that recovered from IR after JTT administration indicated that the terms for immune system process and adaptive immune response (Fig. S4B) were significantly enriched.

Overlapping IR-recovered genes between liver and blood

In addition to organ-specific genes with recovered IR, 11 genes that underwent IR recovery were expressed in both the liver and blood (Fig. 8E, Fig. S5A). Fig. S5B shows the patterns of IR recovery of genes that occurred in both of these organs. Independent occurrence of recovery in different organs strongly suggests the importance of the recovery of these genes for the organism. Among these 11 genes, four splicing-related genes (*Sf3b1*, *Ddx5*, *Srsf5*, and *Srsf6*) were included, again highlighting the importance of the recovery of these genes. Among the remaining seven genes, we paid attention in particular to the following five genes, namely *Nr1h2* (LXRβ), *Faah*, *Gdi1*, *Idh3g*, and *Sh3glb2* (EB2). *Nr1h2* is a key regulator gene in macrophage function (Zelcer and Tontonoz, 2006). *Faah* is connected with macrophage function through lipid metabolism (Xu et al., 2017), and *Gdi1* is connected with interferon-γ activity through innate immunity (Ohshima et al., 2015). *Idh3g* and *Sh3glb2* (EB2) are involved in mitochondrial function (Fino et al., 2017). Considering that one of the prominent functions of JTT has been the activation of the innate immune system, especially macrophage function, the recovery of IR of *Nr1h2* (LXRβ), *Faah*, and *Gdi1* is especially interesting.

Possible involvement of TFs in the increase in retained introns during aging and their decrease by administration of JTT

We first examined enrichment for TF-binding sites in the promoter region spanning 500 bp upstream from the transcription start site in the IR-increased genes in the liver (180 genes, 190 loci) and in the blood (12 genes, 12 loci), categorized as IncIR.KL– vs WT– (Fig. 9A). This type of data shows which TFs were possibly involved in the generation of retained introns that increased during progression of the pre-disease process. Most TFs were organ specific, as only two TFs, SPDEF and Sp1, were shared among genes in both organs, suggesting that they play a more general role in aging. We then examined enrichment for the binding sites of TFs in the IR-recovered genes in the liver (124 genes, 132 loci) and in the blood (39 genes, 40 loci), categorized as DecIR.KL+ vs KL– (Fig. 9B). These data clearly showed that different sets of TFs were used for transcription in IR-recovered genes in liver and in blood. Fig. 9C shows data from Fig. 9A & B for the liver, showing that some TFs were likely involved in both the increase and decrease of retained introns, whereas others were uniquely used in one case or the other.

This observation prompted us to examine how many IR-increased genes or IR-recovered genes in the respective organs have a common TF-binding site in the promoter region spanning 500 bp upstream from the transcription start site. In the case of an increase in IR during aging in the liver, 171 of 180 genes (190 loci) had at least one of four TFs, namely KLF14, SCL, THRb, and Zac1, as shown in Fig. 9D(i)(ii), which represents 95% coverage. In the case of a decrease in retained introns by administration of JTT, 120 of 124 genes (132 loci) had at least one of four TFs, namely SP2, Tgif2, KLF14, and Hoxd12, as shown in Fig. 9E(i)(ii), which represents 96.8% coverage. These data clearly show that a distinct set of genes sharing the same TF-binding sites was chosen during the IR-increasing process of aging and during the IR-decreasing process after administration of JTT and were networked. The significance of this observation will be discussed below.

A similar analysis was performed for the blood data, the results of which are shown in Fig. S6.

Discussion

IR is a marker of the pre-disease state

It has been proposed that retained intron accumulation is a signature for aging (Adusumalli et al., 2019, Huan Li, 2017, Stegeman and Weake, 2017). In the present study, we clearly demonstrated that IR occurs during the pre-disease state when neither pathological alterations nor a difference in protein level could be observed. We speculated that some disruption of homeostasis induced by a change in metabolites triggered IR as a result of a stress during this earlier stage of aging. As shown in Fig. 2A, a significant increase in 3-HBA and decreases in intermediate metabolites of glycolysis in KL– (Fig. 2B) suggest that the liver at this stage is subjected to starvation-like conditions, providing the possibility that this starvation-like state is a stress signal that triggers intron retention. Also, the decrease in 3-HBA in KL+, even if not statistically significant, suggests at least a partial recovery from a starvation-like condition. In addition, metabolome analysis also showed that the concentrations of several nucleotides that are precursors of RNA were lower in KL– (Fig. 2C) relative to that in WT–, suggesting that this also triggered intron retention. It is interesting to note that the concentrations of some of these precursors recovered in KL+ to WT levels. Accordingly, it is possible that the recovery of these precursors after the administration of JTT affected the 180 IR-increased genes to reduce some of these retained introns to the normal state, although this does not necessarily explain the reason why retained introns of only a specific subset of genes were recovered to the normal state by JTT (see the later discussion below).

IR-recovered genes can be classified according to their functions

Fig. 10A illustrates two major categories among the 132 IR-recovered genes, namely alternative splicing and lipid/glucose metabolism. Splicing-related genes such as *Ddx5*, *Sf3b1*, *Srsf5*, and *Srsf6* were included in these IR-recovered genes (Table 2). Splicing-related genes are vulnerable to disruption of homeostasis in many systems, including cancer (Dvinge and Bradley, 2015, Zhang and Manley, 2013), aging (Deschenes and Chabot, 2017), and several stresses (Monteuuis et al., 2019, Shalgi et al., 2014). It is possible that the IR recovery of some of these splicing-related genes reflects the recovery of the normal splicing ability in KL+ after administration of JTT (see the later discussion below).

In addition to genes involved in splicing, retained introns of genes involved in lipid/glucose metabolism such as *Sirt7*, *Decr2*, *Acadm*, *Adipor1*, *Ppard*, *Nr1h2* (*LXRβ*), and *Faah* were recovered (Fig. 10A). They are relevant to hepatic metabolic pathways involving glucose and fatty acids. Under fasting or starvation conditions, endogenous

glucose is mainly produced by a breakdown of glycogen and gluconeogenesis in the liver and is metabolized into pyruvate, which is used to generate ATP through the tricarboxylic acid cycle and oxidative phosphorylation in mitochondria (Nishi et al., 2017). In addition, fatty acids are oxidized through hepatic mitochondrial β-oxidation to generate ketone bodies. Thus, liver-produced glucose and ketone bodies provide essential sources of energy for extrahepatic tissues during fasting and starvation (Rui, 2014). Metabolome analysis showed that the condition of the liver in KL– resembled starvation and that the condition of the liver in KL+ was improved, suggesting that the improvement in the condition of KL+ triggered a cue for the recovery of IR of these genes (see the model proposed below).

In addition to genes belonging to these two categories, a few genes involving mitochondrial processes and immune system and macrophage processes are also included in these IR-recovered genes. These are listed and referenced in the legend of Fig. 10A, in which the possibility is discussed that the IR recovery of several nuclear receptor genes such as *Nr1h2* (LXRβ) might reflect the effect of JTT on macrophage function.

Some liver metabolic functions were improved to the normal state by administration of JTT

Before discussing a model concerning the mechanism by which only certain genes undergo IR recovery in response to JTT, we highlight the results of 213 genes from the DEG analysis, the expression levels of which were down-regulated in KL– and were recovered to the level of WT– in KL+ (Fig.3G). GO analysis of these genes showed that metabolic processes and glucuronidation in the liver likely were up-regulated in KL+ and had recovered after administration of JTT from the down-regulated state in KL– (Fig. 3I).

There are many clinical and basic scientific reports on the improvement of liver functions by JTT, typically exemplified by reports that JTT can protect the liver from injury by chemicals administered to patients with cancer or other diseases. A few examples are listed below (others are listed in the legend for Fig. 10A). JTT protects against isoniazid/rifampicin-induced hepatic injury by modulating oxidative stress and inflammatory responses (Yoshioka et al., 2019). JTT exerts protective effects against alcohol-induced liver disease by modulating oxidative stress and the inflammatory response (Fukaya et al., 2018). JTT has the potential to protect against bromobenzene-induced hepatotoxicity and to modulate oxidative stress (Yoshioka et al., 2016). The

presence of such a variety of reports convinced us that an improvement in liver function, especially metabolic activities, is one of the major effects of JTT. These published data are consistent with our DEG data described above.

A model to explain the reason why IR in a specific subset of genes involving liver metabolism was recovered

As was mentioned in the Introduction, IR has been considered to be harmful to the organism (Weischenfeldt et al., 2005). Recent global screens across many cells and tissue types from humans and mice, however, have gradually revealed the role of IR as a negative regulator of gene expression that is integrated into a regulatory network of RNA processing and has functional significance (Braunschweig et al., 2014, Jacob and Smith, 2017, Liu et al., 2017). Recent studies have shown that programmed IR is a critical regulatory pathway in normal development and differentiation, such as in granulocyte differentiation (Wong et al., 2013), terminal erythroid differentiation (Pimentel et al., 2016), male germ cell differentiation (Naro et al., 2017) and B cell development (Ullrich & Guigo, 2019). The fact that IR within the cyclin A2 gene induces G1/S arrest in differentiated human tissues suggests that IR may play a role in cell differentiation and senescence through regulation of the cell cycle (Honda et al., 2012).

During the heat shock response in mice, there is widespread retention of introns in transcripts from 1,700 genes, which are enriched for tRNA synthetase, nuclear pore, and spliceosome functions. These transcripts with retained introns are, for the most part, nuclear and untranslated. These splicing-inhibited transcripts induced by heat shock stress are mostly spliced post-transcriptionally, in contrast to other normal splicing that occurs co-transcriptionally (Shalgi et al., 2014). These nuclear retained transcripts are presumed to await a signal for splicing that is cued by the release from the stress (Jacob and Smith, 2017). The presence of other similar examples (Boutz et al., 2015, Ninomiya et al., 2011) of stress-induced regulation of intron retention suggests that this regulatory mechanism contributes to a wide range of gene expression.

As aging is also a kind of stress, we considered intron retention during aging as analogous to that which occurs during the heat shock response as described above. Fig. 10C(i) shows a model for the case of KL– in that transcripts with IR are retained in the nucleus upon the stress signal of aging such that global metabolic activity in liver cells is repressed to save energy. After administration of JTT, as liver-specific metabolic functions are recovered to some extent as described above, improvement in metabolic

activity results in a signal to the liver cells to recover these retained introns by sending a cue for post-transcriptional splicing (Fig. 10C(ii)). If this model is correct, we can determine which pathways in the cells are improved by knowing which functions the IR-recovered genes are involved in. In the present case, the recovery of retained introns of genes involved in lipid/glucose metabolic pathways (Fig. 10A) suggests that the liver-specific metabolic functions were recovered. Genes detected by DEG data (Fig. 3F G), the Cten analysis (Fig. 3H), and its GO analysis (Fig. 3I) confirmed that this is the case. Also, the recovery of retained introns of genes involved in splicing pathways (Fig. 8A) suggests that splicing functions were recovered, at least in part. In addition, since a few genes involving mitochondrial processes and immune system and macrophage processes are also included in the IR-recovered genes, we speculate that these functions were also recovered by administration of JTT.

The mechanism for aging-related intron retention in transcripts and possible gene specificity of JTT-related recovery

Regarding the mechanisms related to how transcripts retained their introns and to how a specific group of transcripts was recovered, we suggested above that IR-susceptible genes during aging and IR-recovered genes after JTT administration are transcriptionally controlled by a very few TFs that are specific to the liver and blood (Fig. 9). There is emerging evidence that mRNA splicing is controlled by multi-layered mechanisms that involve transcription and epigenetics (Braunschweig et al., 2014, Lev Maor et al., 2015, Luco et al., 2011). Therefore, it is possible that TFs, chromatin constituents, and epigenetic factors such as those related to histone modification and DNA methylation not only control transcription but also regulate splicing (Lev Maor et al., 2015, Luco et al., 2011). These factors can affect the rate of RNA polymerase II elongation, which in turn affects the pattern of alternative splicing. Accordingly, it is possible that accumulation of retained introns during aging in klotho mice was caused by a change in the elongation rate of transcription. As shown in Fig. 9, there are several TF-binding sites that are enriched in the IR-susceptible genes during aging (190 loci, 180 genes). Accordingly, an aging signal such as fasting may lead specific TFs to retard the transcription rate, resulting in IR. Also, it is possible that some active ingredients of JTT in cooperation with these TFs could contribute to the recovery of IR.

Also, it is interesting to note that the concentration of certain nucleotide diphosphates (UDP and GDP) was decreased in KL– and recovered to WT levels in KL+ (Fig. 3C). If a low concentration of nucleotides triggers a change in the elongation rate of

transcription (Kwak and Lis, 2013), it is also possible that this may have induced the accumulation of retained introns. The recovery of such concentrations to the normal level in KL+ is consistent with the recovery of retained introns in KL+.

Although there are instances in which chemical compounds influence AS by directly interacting with splicing factors (Kataoka, 2017), there has been no report of changes in AS patterns that result from an interaction with a TF. It is of interest to examine whether active ingredients of a Kampo medicine can interact with TFs to influence AS patterns co-transcriptionally or post-transcriptionally. The current results regarding the reduction of retained introns by JTT will provide a rich resource for the subsequent studies of the regulation of AS.

Perspective

This study is the first to shed light on the comprehensive mechanism of a multi-herbal medicine from the viewpoint of systems biology. It is interesting to note that the ancient Chinese medical textbook *Inner Canon of the Yellow Emperor* stated that the pre-disease state should be treated early with Kampo medicine (UNESCO, 2011). The present data represent a molecular proof of this historical statement. Kampo medicine is a precious heritage in Japan, and there are similar medicines used around the world such as traditional Chinese medicines (Patwardhan et al., 2005), traditional medicines in India (Ayurveda) (Patwardhan et al., 2005), and ancient Greek medicines (Unani medicine). To elucidate the mechanisms of these medicines, which are the result of human wisdom that has accumulated over several thousand years, and to pass on this knowledge to subsequent generations are the main goals of our research.

Materials and Methods

Juzen-taiho-to (JTT)

JTT was supplied by Tsumura & Co. (Tokyo, Japan) in the form of a powdered extract. It was obtained by spray-drying a hot water extract mixture of the following 10 crude drugs in the ratios provided in parentheses: Astragali radix (10.52), Cinnamomi cortex (10.52), Rehmanniae radix (10.52), Paeoniae radix (10.52), Cnidii rhizome (10.52), Atractylodis lanceae rhizome (10.52), Angelicae radix (10.52), Ginseng radix (10.52), Poria (10.52), and Glycyrrhizae radix (5.32). The origins and species of each component, the contents of characteristic ingredients, and other pharmaceutical-grade

qualities of JTT are strictly controlled as it is an ethical drug approved by the Ministry of Health, Welfare and Labor of Japan.

RNA extraction and RNA-seq

After removal of organs, they were subjected to RNA extraction after being soaked with RNALater (Thermo Fisher Scientific, Rockford, IL, USA). RNA extraction was performed on individual tissue samples with the Pure Link RNA Mini kit (Invitrogen, MA, USA). Briefly, 600 µL of Lysis Buffer and 900 µL of TRIzol (Thermo Fisher Scientific) were added to 0.03 g of tissue, and the tissue was homogenized. After the sample was incubated for 10 min at room temperature and centrifuged at 12,000 × *g* for 15 min, the supernatant was treated with DNase and purified by column cartridge. The quality of RNA was checked by Qubit (Thermo Fisher Scientific) and TapeStation (Agilent Technologies, CA, USA). RNA library construction was performed by using a TruSeq Stranded mRNA Sample Prep kit (Illumina, CA, USA). Paired-end (150 base pairs × 2) sequencing with the NovaSeq 6000 platform (Illumina) was outsourced to Takara Bio, Shiga, Japan.

Quality check and filtering of RNA-seq data and mapping analysis

For purification of the sequencing data, cutadapt v.1.16 (Deschenes and Chabot, 2017) was used to remove Illumina adapter sequences, followed by removal of the poly(A) sequence using fastx_clipper software in the fastx toolkit software package v.0.0.14 (http://hannonlab.cshl.edu/fastx_toolkit/). To remove low-quality bases or sequences, we trimmed the sequences using fastq_quality_trimmer software (parameters: -t 20 -l 30 -Q 33) and fastq_quality_filter software (parameters: -q 20 -p 80 -Q 33), both of which are included in the fastx toolkit. During the above processing, any read in which one of the pairs was missing was removed using Trimmomatic v.0.38 (Bolger et al., 2014). Then, reads containing mouse rRNA, tRNA, or phiX sequences as the control sequence from Illumina were removed using Bowtie 2 v. 2.3.4.1 (Langmead and Salzberg, 2012). We then carried out the second round of removal of any unpaired reads using bam2fastq. After completion of these filtering steps, 20 million reads of each of the forward and reverse sequences per sample were mapped to the mouse genome sequence build GRCm38 using Tophat v2.1.1 (Trapnell et al., 2009). The mouse genome sequence was downloaded from iGenomes of Illumina (http://jp.support.illumina.com/sequencing/sequencing_software/igenome.html).

679 Multiple mapped reads were removed using samtools (parameters: samtools view -q 4).
680 Uniquely mapped reads were counted by gene annotation (Ensembl release 81) using
681 featureCounts v.1.6.2. The counted values were normalized with the TMM method
682 using EdgeR library in R v.3.5.0 and used for expression analysis.
683
684 **Analysis of alternative splicing**
685
686 Loci with significantly different splicing patterns with $P < 0.01$ were detected within
687 six combinations: KL+/KL–, KL+/WT+, KL+/WT–, KL–/WT+, KL–/WT–, and
688 WT+/WT–, where '+' and '–' refer to treatment with and without, respectively, JTT,
689 using rMATS v.4.0.2 (Shen et al., 2014). Statistical significance was tested using the
690 skipping junction counts (SJCs) and the inclusion junction counts (IJCs) as calculated
691 by rMATS at the corresponding loci. We checked the mapping status and generated the
692 mapping result view using IGV (http://software.broadinstitute.org/software/igv/)
693 (Robinson et al., 2011).
694
695 **Analysis of characteristics for the IR gene group**
696
697 We analyzed enriched gene functions and pathways at 142 loci (134 genes) at which
698 significantly different IR events were detected between KL+ and KL– using DAVID ver
699 6.8 (https://david.ncifcrf.gov/) (Huang da et al., 2009) with the following criteria: Count
700 ≥ 1, EASE ≤ 1.
701
702 **Splice site score**
703
704 For the evaluation of splice site strength, maximum entropy scores for 5' and 3' splice
705 sites were calculated using MaxEntScan (Yeo and Burge, 2004).
706
707 **Motif analysis**
708
709 For the comparison of protein-binding motifs in the mRNA, we compared motifs with
710 the ATtRACT database of RNA-biding proteins and their associated motifs (Giudice et
711 al., 2016). We compared TF-binding sites using HOMER (Heinz et al., 2010) with
712 default parameters. All detected motifs were then compared using Fisher's test.
713
714 **Definition of potential splicing-related genes**

The KEGG pathway lists ~140 proteins as spliceosomal proteins, and we then added 109 genes from the Gene Ontology (GO) list (GO:0000398) of mRNA splicing via spliceosome. We also added 66 genes from the GO list (GO:0003729) of mRNA binding and 180 genes from the GO list (GO:0006397) of mRNA processing, both of which were chosen to overlap with genes listed by Han et al. (2017) that were selected based on the criterion that a knock-down experiment influenced their alternative splicing. After removing duplicates, we ultimately defined 250 genes as potential splicing-related genes in this analysis. They included almost all the spliceosomal proteins and spliceosome regulatory proteins.

Reverse transcription PCR amplification of IR loci

The extracted RNA was treated with Recombinant DNase I (Takara Bio, Japan) to digest the remaining genomic DNA and was purified by phenol/chloroform/isoamyl alcohol (25:24:21) and ethanol precipitation. The purified RNA was reverse transcribed using High-Capacity cDNA Reverse Transcription kits (Thermo Fisher Scientific). Primers were prepared in exons adjacent to the IR locus, and PCR amplification was performed using the cDNA. Reaction conditions were as follows: 5 μL 10× PCR buffer (Takara Bio), 5 μL dNTPs (25 mM; Takara Bio), 1 μL primers (10 pmol/μL each primer), 0.2 μL ExTaq DNA polymerase (5 U/μL; Takara Bio), 40 ng of template DNA, and DNase-free water added to a final volume of 50 μL. PCR was performed using GeneAmp PCR system 9700 (Thermo Fisher Scientific) with the following conditions: initial annealing at 96°C for 5 min, followed by 25 or 30 cycles (96ºC for 30 sec, 55ºC for 45 sec, 72ºC for 2 min). After a final extension at 72°C for 5 min, the PCR mixtures were held at 4°C. The amplicon was confirmed based on size by TapeStation. The primer set used is listed in supplementary information (SI). Primer sequences were listed in Table S1.

Analysis of DEG

Genes that had significantly differential expression with $P < 0.01$ in two comparisons, namely KL+/KL– and KL–/WT–, were detected using edgeR (Robinson et al., 2010). The recovered genes that were significantly down-regulated in KL– as compared with WT– and significantly up-regulated in KL+ as compared with KL– were extracted.

Western blot analysis

Mouse liver samples were homogenized in ice-cold RIPA buffer (50 mM Tris, 150 mM NaCl, 1% NP-40, 0.5% deoxycholic acid sodium monohydrate, 0.1% SDS, 10 mM NaF, pH 7.4) with a Disposable homogenizer (Nippi BioMasher) (30 strokes), and the homogenates were centrifuged at 10,000 × *g* and 4°C for 20 min. The protein concentration of each supernatant was measured by the BCA protein assay (Thermo Fisher Scientific), and supernatants were diluted to equal protein concentrations, combined with 2 M DTT (final concentration, 0.2 M) and 4× SDS sample buffer (6% SDS, 40% glycerol, 0.4% bromophenol blue, 250 mM Tris, pH 6.8), and boiled for 5 min at 95°C.

Protein samples (30 μg/well) were resolved by SDS-PAGE and then transferred onto PVDF membranes. The membranes were blocked with 5% milk in TBST (20 mM Tris, 150 mM NaCl, containing 0.05% Tween-20, pH 7.4) and incubated with primary antibodies at 4°C overnight. Primary antibodies used in this study were anti-RGN/SMP30 (17947-1-AP, Proteintech), anti-DDX5,p68 (10804-1-AP, Proteintech), anti-NDUFS2 (GTX114924, GeneTex), anti-PPARD (10156-2-AP, Proteintech), anti-SIRT7 (12994-1-AP, Proteintech), anti-NXF1 (10328-1-AP, Proteintech), anti-SRSF6 (11772-1-AP, Proteintech), anti-LXR beta (ab28479, Abcam), and anti-GAPDH (sc-32233, Santa Cruz Biotechnology). After incubation with secondary antibodies peroxidase-conjugated anti–rabbit IgG (SA00001-2, Proteintech) or anti–mouse IgG (sc-516102, Santa Cruz Biotechnology), protein bands were detected using ECL Prime Western Blotting Detection Reagents (GE Healthcare). Some of the membranes were probed with anti-GAPDH , which was used as the loading control for other blots in each experiment. The signal intensity was quantified using ImageJ (NIH) or a ChemiDoc system (Bio-Rad). Western blots were repeated a minimum of three times with different animals, and representative blots are shown.

Data availability

The original RNA-seq datasets have been deposited in the DDBJ Sequence Read Archive under accession numbers DRR167982–DRR167990, which are linked to the BioProject accession number PRJDB7898.

Acknowledgements

The present work was financially supported by FAIS and Zenick Co. represented by Mr. Y. Otake and Mr. T. Sugino, respectively. We thank Mr. K. Onodera for management and discussions and Ms. A. Koizumi for making illustrations.

Competing interests

N.O., K.O., Y.I., A.M., E.I., T.V., and S.N., received a research grant from Zenick Co. and Tsumura & Co. N.F., A.N., A.S., M.N., A.K., and M.Y. are employees of Tsumura & Co.

References

1. Adusumalli, S., Ngian, Z.K., Lin, W.Q., Benoukraf, T., and Ong, C.T. (2019). Increased intron retention is a post-transcriptional signature associated with progressive aging and Alzheimer's disease. *Aging Cell* **18**(3), e12928. DOI: 10.1111/acel.12928.
2. Bolger, A.M., Lohse, M., and Usadel, B. (2014). Trimmomatic: a flexible trimmer for Illumina sequence data. *Bioinformatics* **30**(15), 2114-2120. DOI: 10.1093/bioinformatics/btu170.
3. Boutz, P.L., Bhutkar, A., and Sharp, P.A. (2015). Detained introns are a novel, widespread class of post-transcriptionally spliced introns. *Genes Dev* **29**(1), 63-80. DOI: 10.1101/gad.247361.114.
4. Braunschweig, U., Barbosa-Morais, N.L., Pan, Q., Nachman, E.N., Alipanahi, B., Gonatopoulos-Pournatzis, T., Frey, B., Irimia, M., and Blencowe, B.J. (2014). Widespread intron retention in mammals functionally tunes transcriptomes. *Genome Res* **24**(11), 1774-1786. DOI: 10.1101/gr.177790.114.
5. Deschenes, M., and Chabot, B. (2017). The emerging role of alternative splicing in senescence and aging. *Aging Cell* **16**(5), 918-933. DOI: 10.1111/acel.12646.
6. Dvinge, H., and Bradley, R.K. (2015). Widespread intron retention diversifies most cancer transcriptomes. *Genome Med* **7**(1), 45. DOI: 10.1186/s13073-015-0168-9.
7. Dvinge, H., Kim, E., Abdel-Wahab, O., and Bradley, R.K. (2016). RNA splicing factors as oncoproteins and tumour suppressors. *Nat Rev Cancer* **16**(7), 413-430. DOI: 10.1038/nrc.2016.51.

8. Fino, K.K., Yang, L., Silveyra, P., Hu, S., Umstead, T.M., DiAngelo, S., Halstead, E.S., Cooper, T.K., Abraham, T., Takahashi, Y., *et al.* (2017). SH3GLB2/endophilin B2 regulates lung homeostasis and recovery from severe influenza A virus infection. *Scientific Reports* **7**(1), 7262. DOI: 10.1038/s41598-017-07724-5.

9. Fouache, A., Zabaiou, N., De Joussineau, C., Morel, L., Silvente-Poirot, S., Namsi, A., Lizard, G., Poirot, M., Makishima, M., Baron, S., *et al.* (2019). Flavonoids differentially modulate liver X receptors activity-Structure-function relationship analysis. *J Steroid Biochem Mol Biol* **190**, 173-182. DOI: 10.1016/j.jsbmb.2019.03.028.

10. Fukao, T., Mitchell, G., Sass, J.O., Hori, T., Orii, K., and Aoyama, Y. (2014). Ketone body metabolism and its defects. *J Inherit Metab Dis* **37**(4), 541-551. DOI: 10.1007/s10545-014-9704-9.

11. Fukaya, S., Nagatsu, A., and Yoshioka, H. (2018). The Kampo formula "Juzen-taiho-to" exerts protective effects on ethanol -induced liver injury mice. *Fundamental Toxicological Sciences* **5**(3), 105-112. DOI: doi:10.2131/fts.5.105

12. Giudice, G., Sanchez-Cabo, F., Torroja, C., and Lara-Pezzi, E. (2016). ATtRACT-a database of RNA-binding proteins and associated motifs. *Database (Oxford)* **2016**. DOI: 10.1093/database/baw035.

13. Han, H., Braunschweig, U., Gonatopoulos-Pournatzis, T., Weatheritt, R.J., Hirsch, C.L., Ha, K.C.H., Radovani, E., Nabeel-Shah, S., Sterne-Weiler, T., Wang, J., *et al.* (2017). Multilayered Control of Alternative Splicing Regulatory Networks by Transcription Factors. *Mol Cell* **65**(3), 539-553 e537. DOI: 10.1016/j.molcel.2017.01.011.

14. Heinz, S., Benner, C., Spann, N., Bertolino, E., Lin, Y.C., Laslo, P., Cheng, J.X., Murre, C., Singh, H., and Glass, C.K. (2010). Simple combinations of lineage-determining transcription factors prime cis-regulatory elements required for macrophage and B cell identities. *Mol Cell* **38**(4), 576-589. DOI: 10.1016/j.molcel.2010.05.004.

15. Honda, A., Valogne, Y., Bou Nader, M., Brechot, C., and Faivre, J. (2012). An intron-retaining splice variant of human cyclin A2, expressed in adult differentiated tissues, induces a G1/S cell cycle arrest in vitro. *PLoS One* **7**(6), e39249. DOI: 10.1371/journal.pone.0039249.

16. Huan Li, Z.W., Tianyi Ma, Gang Wei, Ting Ni (2017). Alternative splicing in aging and age-related diseases. *Translational Medicine of Aging* **1**, 32-40. DOI, https://www.sciencedirect.com/science/article/pii/S246850111730007X.

17. Huang da, W., Sherman, B.T., and Lempicki, R.A. (2009). Systematic and integrative analysis of large gene lists using DAVID bioinformatics resources. *Nat Protoc* **4**(1), 44-57. DOI: 10.1038/nprot.2008.211.

18. Ishikawa, S., Ishikawa, T., Tezuka, C., Asano, K., Sunagawa, M., and Hisamitsu, T. (2017). Efficacy of Juzentaihoto for Tumor Immunotherapy in B16 Melanoma Metastasis Model. *Evid Based Complement Alternat Med* **2017**, 6054706. DOI: 10.1155/2017/6054706.

19. Jacob, A.G., and Smith, C.W.J. (2017). Intron retention as a component of regulated gene expression programs. *Hum Genet* **136**(9), 1043-1057. DOI: 10.1007/s00439-017-1791-x.

20. Kaneko, A., Matsumoto, T., Matsubara, Y., Sekiguchi, K., Koseki, J., Yakabe, R., Aoki, K., Aiba, S., and Yamasaki, K. (2017). Glucuronides of phytoestrogen flavonoid enhance macrophage function via conversion to aglycones by beta-glucuronidase in macrophages. *Immun Inflamm Dis* **5**(3), 265-279. DOI: 10.1002/iid3.163.

21. Kataoka, N. (2017). Modulation of aberrant splicing in human RNA diseases by chemical compounds. *Hum Genet* **136**(9), 1237-1245. DOI: 10.1007/s00439-017-1789-4.

22. Kitamura, K., Iino, Y., Kamide, Y., Kudo, F., Nakayama, T., Suzuki, K., Taiji, H., Takahashi, H., Yamanaka, N., and Uno, Y. (2015). Clinical practice guidelines for the diagnosis and management of acute otitis media (AOM) in children in Japan - 2013 update. *Auris Nasus Larynx* **42**(2), 99-106. DOI: 10.1016/j.anl.2014.09.006.

23. Ko, J.H., Lee, J.H., Choi, B., Park, J.Y., Kwon, Y.W., Jeon, S., Park, S.D., and Kim, S.N. (2018). Neuroprotective Effects of Gagam-Sipjeondaebo-Tang, a Novel Herbal Formula, against MPTP-Induced Parkinsonian Mice and MPP(+)-Induced Cell Death in SH-SY5Y Cells. *Evid Based Complement Alternat Med* **2018**, 2420809. DOI: 10.1155/2018/2420809.

24. Kuro-o, M., Matsumura, Y., Aizawa, H., Kawaguchi, H., Suga, T., Utsugi, T., Ohyama, Y., Kurabayashi, M., Kaname, T., Kume, E.*, et al.* (1997). Mutation of the mouse klotho gene leads to a syndrome resembling ageing. *Nature* **390**(6655), 45-51. DOI: 10.1038/36285.

25. Kwak, H., and Lis, J.T. (2013). Control of transcriptional elongation. *Annu Rev Genet* **47**, 483-508. DOI: 10.1146/annurev-genet-110711-155440.

26. Langmead, B., and Salzberg, S.L. (2012). Fast gapped-read alignment with Bowtie 2. *Nat Methods* **9**(4), 357-359. DOI: 10.1038/nmeth.1923.

27. Lejeune, F., and Maquat, L.E. (2005). Mechanistic links between nonsense-

mediated mRNA decay and pre-mRNA splicing in mammalian cells. *Curr Opin Cell Biol* **17**(3), 309-315. DOI: 10.1016/j.ceb.2005.03.002.

28. Lev Maor, G., Yearim, A., and Ast, G. (2015). The alternative role of DNA methylation in splicing regulation. *Trends Genet* **31**(5), 274-280. DOI: 10.1016/j.tig.2015.03.002.

29. Liu, Y., Gonzalez-Porta, M., Santos, S., Brazma, A., Marioni, J.C., Aebersold, R., Venkitaraman, A.R., and Wickramasinghe, V.O. (2017). Impact of Alternative Splicing on the Human Proteome. *Cell Rep* **20**(5), 1229-1241. DOI: 10.1016/j.celrep.2017.07.025.

30. Lopez-Otin, C., Blasco, M.A., Partridge, L., Serrano, M., and Kroemer, G. (2013). The hallmarks of aging. *Cell* **153**(6), 1194-1217. DOI: 10.1016/j.cell.2013.05.039.

31. Luco, R.F., Allo, M., Schor, I.E., Kornblihtt, A.R., and Misteli, T. (2011). Epigenetics in alternative pre-mRNA splicing. *Cell* **144**(1), 16-26. DOI: 10.1016/j.cell.2010.11.056.

32. Maruyama, N., Ishigami, A., and Kondo, Y. (2010). Pathophysiological significance of senescence marker protein-30. *Geriatr Gerontol Int* **10 Suppl 1**, S88-98. DOI: 10.1111/j.1447-0594.2010.00586.x.

33. Matsumoto, T., Sakurai, M.H., Kiyohara, H., and Yamada, H. (2000). Orally administered decoction of Kampo (Japanese herbal) medicine, "Juzen-Taiho-To" modulates cytokine secretion and induces NKT cells in mouse liver. *Immunopharmacology* **46**(2), 149-161. DOI: 10.1016/S0162-3109(99)00166-6.

34. Mayeda, A., Munroe, S.H., Caceres, J.F., and Krainer, A.R. (1994). Function of conserved domains of hnRNP A1 and other hnRNP A/B proteins. *EMBO J* **13**(22), 5483-5495. DOI: 10.1002/j.1460-2075.1994.tb06883.x

35. Monteuuis, G., Wong, J.J.L., Bailey, C.G., Schmitz, U., and Rasko, J.E.J. (2019). The changing paradigm of intron retention: regulation, ramifications and recipes. *Nucleic Acids Res* **47**(22), 11497-11513. DOI: 10.1093/nar/gkz1068.

36. Munakata, K., Takashima, K., Nishiyama, M., Asano, N., Mase, A., Hioki, K., Ohnishi, Y., Yamamoto, M., and Watanabe, K. (2012). Microarray analysis on germfree mice elucidates the primary target of a traditional Japanese medicine juzentaihoto: acceleration of IFN-alpha response via affecting the ISGF3-IRF7 signaling cascade. *BMC Genomics* **13**, 30. DOI: 10.1186/1471-2164-13-30.

37. Naro, C., Jolly, A., Di Persio, S., Bielli, P., Setterblad, N., Alberdi, A.J., Vicini, E., Geremia, R., De la Grange, P., and Sette, C. (2017). An Orchestrated Intron Retention Program in Meiosis Controls Timely Usage of Transcripts during Germ Cell Differentiation. *Dev Cell* **41**(1), 82-93 e84. DOI:

10.1016/j.devcel.2017.03.003.

38. Niemela, E.H., Oghabian, A., Staals, R.H., Greco, D., Pruijn, G.J., and Frilander, M.J. (2014). Global analysis of the nuclear processing of transcripts with unspliced U12-type introns by the exosome. *Nucleic Acids Res* **42**(11), 7358-7369. DOI: 10.1093/nar/gku391.

39. Ninomiya, K., Kataoka, N., and Hagiwara, M. (2011). Stress-responsive maturation of Clk1/4 pre-mRNAs promotes phosphorylation of SR splicing factor. *J Cell Biol* **195**(1), 27-40. DOI: 10.1083/jcb.201107093.

40. Nishi, A., Ohbuchi, K., Kushida, H., Matsumoto, T., Lee, K., Kuroki, H., Nabeshima, S., Shimobori, C., Komokata, N., Kanno, H., *et al.* (2017). Deconstructing the traditional Japanese medicine "Kampo": compounds, metabolites and pharmacological profile of maoto, a remedy for flu-like symptoms. *NPJ Syst Biol Appl* **3**, 32. DOI: 10.1038/s41540-017-0032-1.

41. Ohshima, J., Sasai, M., Liu, J., Yamashita, K., Ma, J.S., Lee, Y., Bando, H., Howard, J.C., Ebisu, S., Hayashi, M., *et al.* (2015). RabGDIalpha is a negative regulator of interferon-gamma-inducible GTPase-dependent cell-autonomous immunity to Toxoplasma gondii. *Proc Natl Acad Sci U S A* **112**(33), E4581-4590. DOI: 10.1073/pnas.1510031112.

42. Okumi, H., and Koyama, A. (2014). Kampo medicine for palliative care in Japan. *Biopsychosoc Med* **8**(1), 6. DOI: 10.1186/1751-0759-8-6.

43. Onishi, Y., Yamaura, T., Tauchi, K., Sakamoto, T., Tsukada, K., Nunome, S., Komatsu, Y., and Saiki, I. (1998). Expression of the anti-metastatic effect induced by Juzen-taiho-to is based on the content of Shimotsu-to constituents. *Biol Pharm Bull* **21**(7), 761-765. DOI: 10.1248/bpb.21.761.

44. Padgett, R.A., Grabowski, P.J., Konarska, M.M., Seiler, S., and Sharp, P.A. (1986). Splicing of messenger RNA precursors. *Annu Rev Biochem* **55**, 1119-1150. DOI: 10.1146/annurev.bi.55.070186.005351.

45. Park, S.M., Kim, S.W., Jung, E.H., Ko, H.L., Im, C.K., Lee, J.R., Byun, S.H., Ku, S.K., Kim, S.C., Park, C.A., *et al.* (2018). Sipjeondaebo-tang Alleviates Oxidative Stress-Mediated Liver Injury through Activation of the CaMKK2-AMPK Signaling Pathway. *Evid Based Complement Alternat Med* **2018**, 8609285. DOI: 10.1155/2018/8609285.

46. Patel, A.A., and Steitz, J.A. (2003). Splicing double: insights from the second spliceosome. *Nat Rev Mol Cell Biol* **4**(12), 960-970. DOI: 10.1038/nrm1259.

47. Patwardhan, B., Warude, D., Pushpangadan, P., and Bhatt, N. (2005). Ayurveda and traditional Chinese medicine: a comparative overview. *Evid Based*

Complement Alternat Med **2**(4), 465-473. DOI: 10.1093/ecam/neh140.

48. Pimentel, H., Parra, M., Gee, S.L., Mohandas, N., Pachter, L., and Conboy, J.G. (2016). A dynamic intron retention program enriched in RNA processing genes regulates gene expression during terminal erythropoiesis. *Nucleic Acids Res* **44**(2), 838-851. DOI: 10.1093/nar/gkv1168.

49. Razzaque, M.S. (2009). The FGF23-Klotho axis: endocrine regulation of phosphate homeostasis. *Nat Rev Endocrinol* **5**(11), 611-619. DOI: 10.1038/nrendo.2009.196.

50. Robinson, J.T., Thorvaldsdottir, H., Winckler, W., Guttman, M., Lander, E.S., Getz, G., and Mesirov, J.P. (2011). Integrative genomics viewer. *Nat Biotechnol* **29**(1), 24-26. DOI: 10.1038/nbt.1754.

51. Robinson, M.D., McCarthy, D.J., and Smyth, G.K. (2010). edgeR: a Bioconductor package for differential expression analysis of digital gene expression data. *Bioinformatics* **26**(1), 139-140. DOI: 10.1093/bioinformatics/btp616.

52. Rui, L. (2014). Energy metabolism in the liver. *Compr Physiol* **4**(1), 177-197. DOI: 10.1002/cphy.c130024.

53. Saiki, I. (2000). A Kampo medicine "Juzen-taiho-to"--prevention of malignant progression and metastasis of tumor cells and the mechanism of action. *Biol Pharm Bull* **23**(6), 677-688. DOI: 10.1248/bpb.23.677.

54. Saiki, I., Koizumi, K., Goto, H., Inujima, A., Namiki, T., Raimura, M., Kogure, T., Tatsumi, T., Inoue, H., Sakai, S.*, et al.* (2013). The long-term effects of a kampo medicine, juzentaihoto, on maintenance of antibody titer in elderly people after influenza vaccination. *Evid Based Complement Alternat Med* **2013**, 568074. DOI: 10.1155/2013/568074.

55. Shalgi, R., Hurt, J.A., Lindquist, S., and Burge, C.B. (2014). Widespread inhibition of posttranscriptional splicing shapes the cellular transcriptome following heat shock. *Cell Rep* **7**(5), 1362-1370. DOI: 10.1016/j.celrep.2014.04.044.

56. Shen, S., Park, J.W., Lu, Z.X., Lin, L., Henry, M.D., Wu, Y.N., Zhou, Q., and Xing, Y. (2014). rMATS: robust and flexible detection of differential alternative splicing from replicate RNA-Seq data. *Proc Natl Acad Sci U S A* **111**(51), E5593-5601. DOI: 10.1073/pnas.1419161111.

57. Shoemaker, J.E., Lopes, T.J.S., Ghosh, S., Matsuoka, Y., Kawaoka, Y., and Kitano, H. (2012). CTen: a web-based platform for identifying enriched cell types from heterogeneous microarray data. *BMC Genomics* **13**(1), 460. DOI: 10.1186/1471-2164-13-460.

58. Solana, R., Pawelec, G., and Tarazona, R. (2006). Aging and innate immunity.

Immunity **24**(5), 491-494. DOI: 10.1016/j.immuni.2006.05.003.

59. Stegeman, R., and Weake, V.M. (2017). Transcriptional Signatures of Aging. *J Mol Biol* **429**(16), 2427-2437. DOI: 10.1016/j.jmb.2017.06.019.

60. Takeno, N., Inujima, A., Shinohara, K., Yamada, M., Shibahara, N., Sakurai, H., Saiki, I., and Koizumi, K. (2015). Immune adjuvant effect of Juzentaihoto, a Japanese traditional herbal medicine, on tumor vaccine therapy in a mouse model. *Int J Oncol* **47**(6), 2115-2122. DOI: 10.3892/ijo.2015.3208.

61. Trapnell, C., Pachter, L., and Salzberg, S.L. (2009). TopHat: discovering splice junctions with RNA-Seq. *Bioinformatics* **25**(9), 1105-1111. DOI: 10.1093/bioinformatics/btp120.

62. Ullrich, S., and Guigo, R. (2019). Dynamic changes in intron retention are tightly associated with regulation of splicing factors and proliferative activity during B-cell development. *Nucleic Acids Res*. DOI: 10.1093/nar/gkz1180.

63. UNESCO (2011). Huang Di Nei Jing (Yellow Emperor's Inner Canon) (Beijing: National Library of China).

64. Vu, T.-D., Iwasaki, Y., Shigenobu, S., Maruko, A., Oshima, K., Iioka, E., Huang, C-L. Abe, T., Tamaki, S., Lin, Y-W., Chen, C-K., Lu, M-Y., Hojo, M., Wang, H-V., Tzeng, S-F., Huang, H-J., Kanai, A,, Gojobori, T., Chiang, T-Y., Sun, H.S., Li, W-H., Okada, N. (2019). Behavioral and neurotranscriptomic synchronization between the two opponents of a fighting pair of the fish Betta splendens. *PLOS Biology.* submitted.

65. Wang, Z., Qi, F., Cui, Y., Zhao, L., Sun, X., Tang, W., and Cai, P. (2018). An update on Chinese herbal medicines as adjuvant treatment of anticancer therapeutics. *Biosci Trends* **12**(3), 220-239. DOI: 10.5582/bst.2018.01144.

66. Weischenfeldt, J., Lykke-Andersen, J., and Porse, B. (2005). Messenger RNA surveillance: neutralizing natural nonsense. *Curr Biol* **15**(14), R559-562. DOI: 10.1016/j.cub.2005.07.002.

67. Wong, J.J., Ritchie, W., Ebner, O.A., Selbach, M., Wong, J.W., Huang, Y., Gao, D., Pinello, N., Gonzalez, M., Baidya, K.*, et al.* (2013). Orchestrated intron retention regulates normal granulocyte differentiation. *Cell* **154**(3), 583-595. DOI: 10.1016/j.cell.2013.06.052.

68. Xu, W., Wei, Z., Dong, J., Duan, F., Chen, K., Chen, C., Liu, J., Yang, X., Chen, L., Xiao, H.*, et al.* (2017). Global Metabolomics Reveals the Metabolic Dysfunction in Ox-LDL Induced Macrophage-Derived Foam Cells. *Front Pharmacol* **8**, 586. DOI: 10.3389/fphar.2017.00586.

69. Yeo, G., and Burge, C.B. (2004). Maximum entropy modeling of short sequence

motifs with applications to RNA splicing signals. *J Comput Biol* **11**(2-3), 377-394. DOI: 10.1089/1066527041410418.

70. Yoshioka, H., Fukaya, S., Miura, N., Nagatsu, A., and Nonogaki, T. (2016). Hepatoprotective effect of kampo formula "Juzen-taiho-to" on bromobenzene-induced toxicity in mice. *Fundamental Toxicological Sciences* **3**(5), 233-236. DOI: 10.2131/fts.3.233.

71. Yoshioka, H., Fukaya, S., Tominaga, S., Nagatsu, A., Miura, N., and Maeda, T. (2019). Protective effect of the Kampo formula "Juzen-taiho-to" on isoniazid- and rifampicin-induced hepatotoxicity in mice. *Fundamental Toxicological Sciences* **6**(1), 25-29. DOI: 10.2131/fts.6.25.

72. Zane, L., Sharma, V., and Misteli, T. (2014). Common features of chromatin in aging and cancer: cause or coincidence? *Trends Cell Biol* **24**(11), 686-694. DOI: 10.1016/j.tcb.2014.07.001.

73. Zelcer, N., and Tontonoz, P. (2006). Liver X receptors as integrators of metabolic and inflammatory signaling. *J Clin Invest* **116**(3), 607-614. DOI: 10.1172/JCI27883.

74. Zhang, J., and Manley, J.L. (2013). Misregulation of pre-mRNA alternative splicing in cancer. *Cancer Discov* **3**(11), 1228-1237. DOI: 10.1158/2159-8290.CD-13-0253.

75. Zheng, H.C., Noguchi, A., Kikuchi, K., Ando, T., Nakamura, T., and Takano, Y. (2014). Gene expression profiling of lens tumors, liver and spleen in alpha-crystallin/SV40 T antigen transgenic mice treated with Juzen-taiho-to. *Mol Med Rep* **9**(2), 547-552. DOI: 10.3892/mmr.2013.1854.

76. Zhou, X., Seto, S.W., Chang, D., Kiat, H., Razmovski-Naumovski, V., Chan, K., and Bensoussan, A. (2016). Synergistic Effects of Chinese Herbal Medicine: A Comprehensive Review of Methodology and Current Research. *Front Pharmacol* **7**, 201. DOI: 10.3389/fphar.2016.00201.

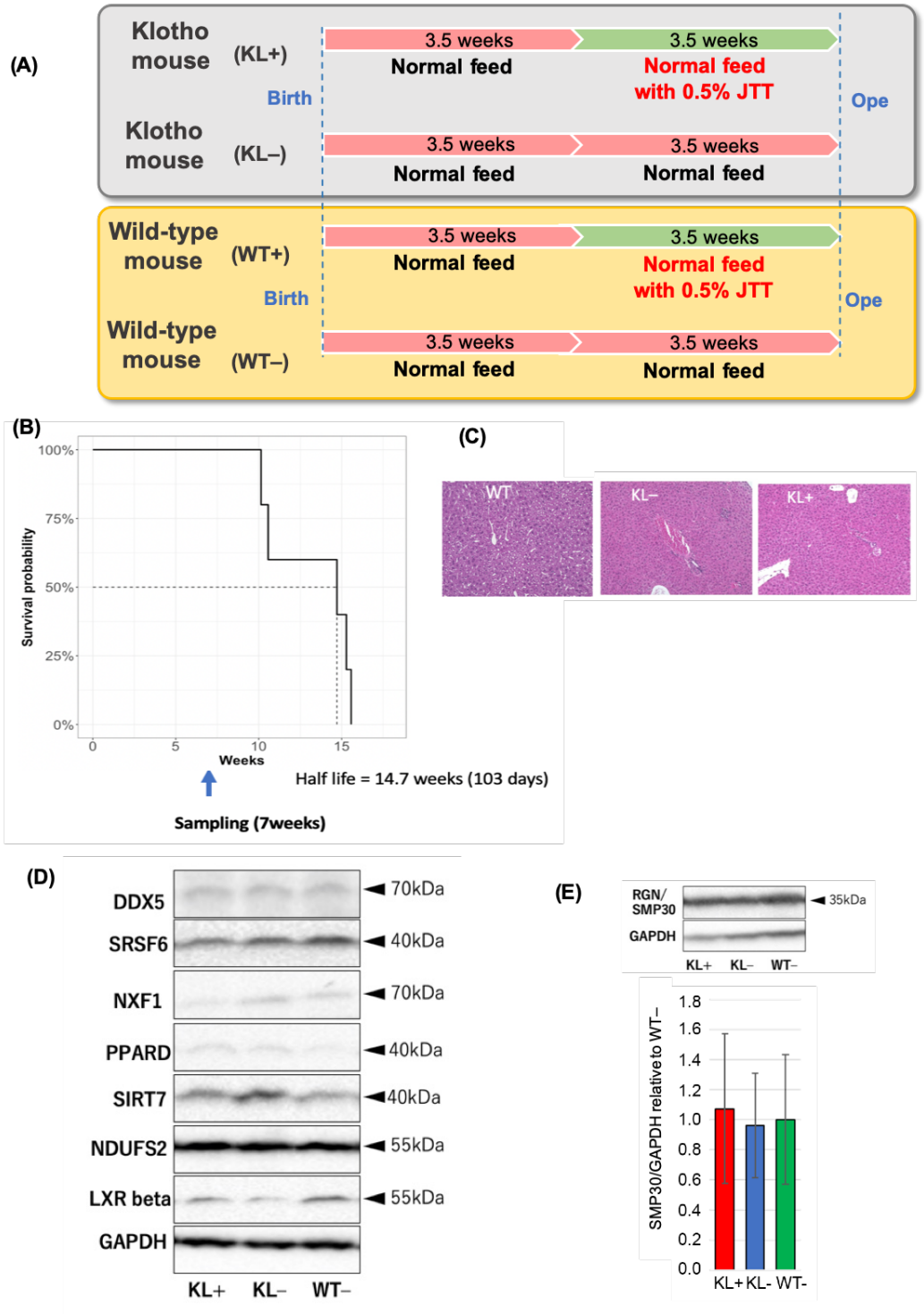

Figure 1. Klotho mice at 7 weeks of age represent the pre-disease state

(A) Schematic illustration of animal experiments. Three-week-old male α-klotho knockout (*Kl*$^{-/-}$/Jcl) mice (klotho mice) (n = 8) and WT (C57BL/6JJcl) mice (n = 8) were purchased from CLEA Japan, Tokyo, Japan. The mice were acclimated for 0.5 weeks in a vinyl isolator, during which they were given radiation-sterilized water and

CE-2 diet (CLEA Japan) ad libitum. Thereafter, the klotho mice and WT mice were each divided into two groups, with four animals in each. In each case, one group of mice was fed CE-2 containing 0.5% (w/w) JTT, whereas the other group was fed CE-2 only from 3.5 weeks of age until the mice were 7 weeks old. Ope stands for operation. (B) Estimation of the half-life of klotho mice. N = 5. (C) Histological observations of liver tissues from KL+ and KL– showed that they did not exhibit any signs of aging relative to WT mice. (D) The expression of seven proteins, each of which showed IR, was examined by western blotting. Expression levels did not change in KL+, KL–, and WT– at 7 weeks of age. (E) Representative western blotting data (upper) of a senescence marker protein, RGN/SMP30, together with its quantified expression (lower) show that KL– are not senescent. Statistical significance was estimated by one-way ANOVA. Error bars indicate mean ±standard deviations of triplicate measurements.

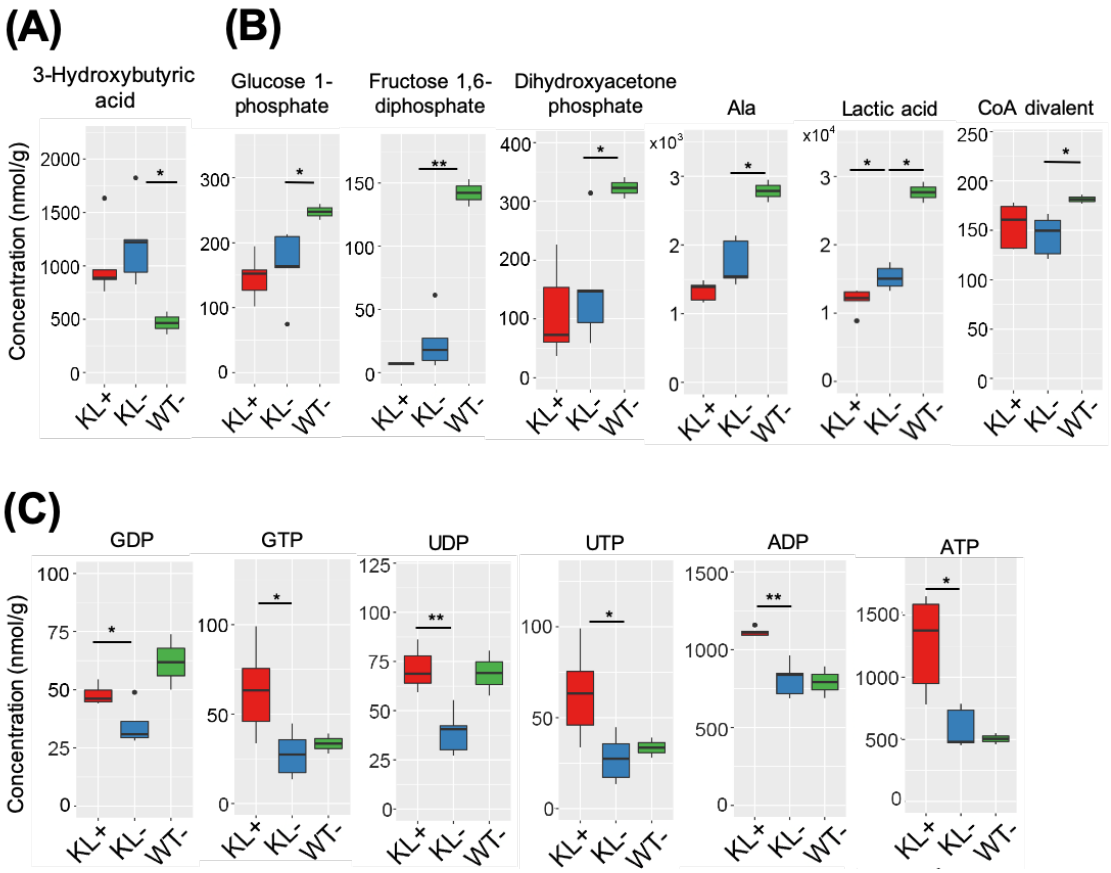

Figure 2. A metabolome analysis showed that the klotho mice are undergoing a starvation-like condition at 7 weeks of age

Based on a metabolome analysis of (A) 3-HBA and (B) other glycolysis-related metabolites, KL– data indicate that these mice are undergoing a starvation-like condition. *P ≤ 0.05, **P ≤ 0.001, unpaired Student's t-test. Based on the metabolome analysis about metabolites related to RNA precursors, the concentrations of some nucleotides were recovered in KL+ in comparison with KL– and WT–. *P ≤ 0.05, **P ≤ 0.001, unpaired Student's t-test.

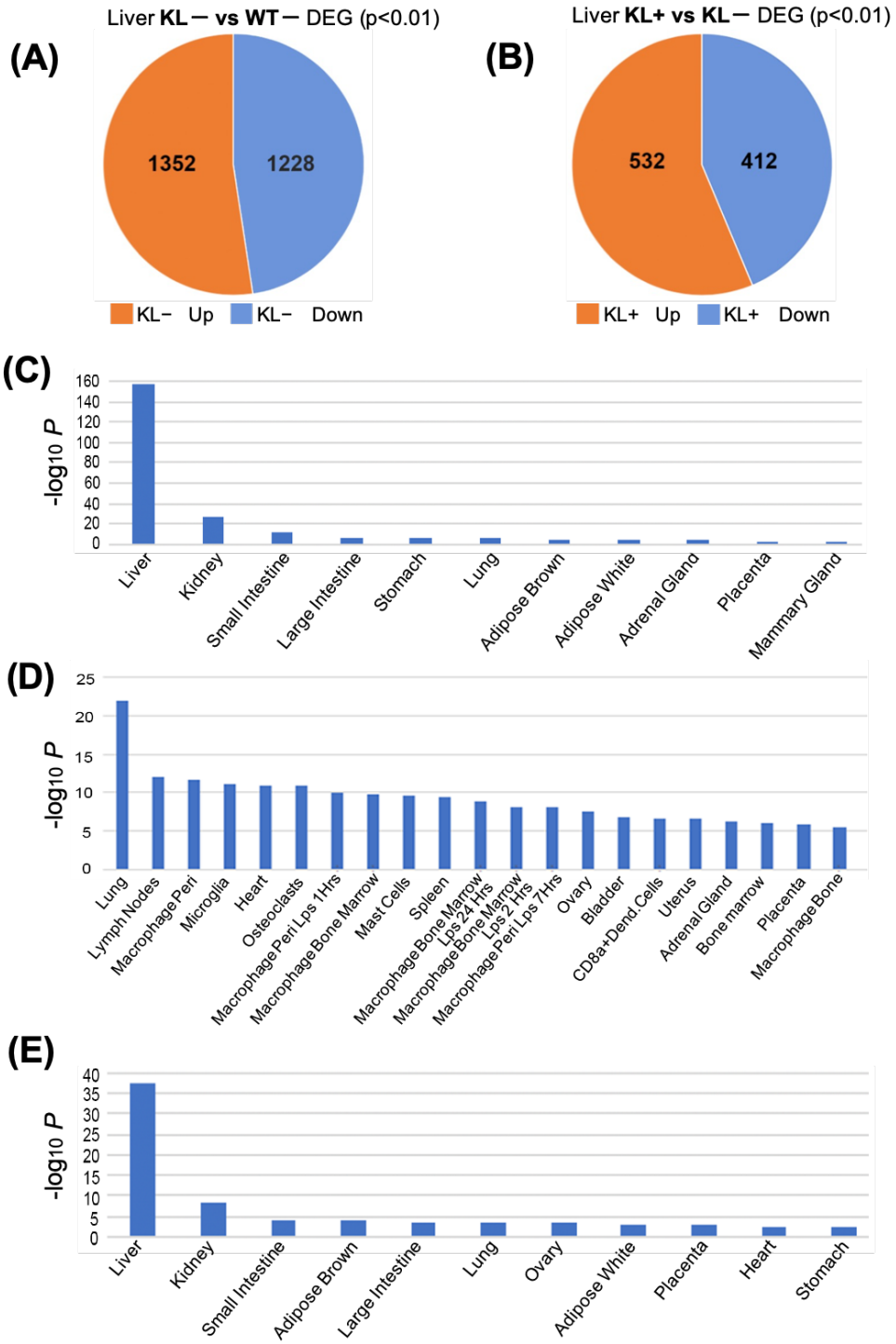

1101
1102

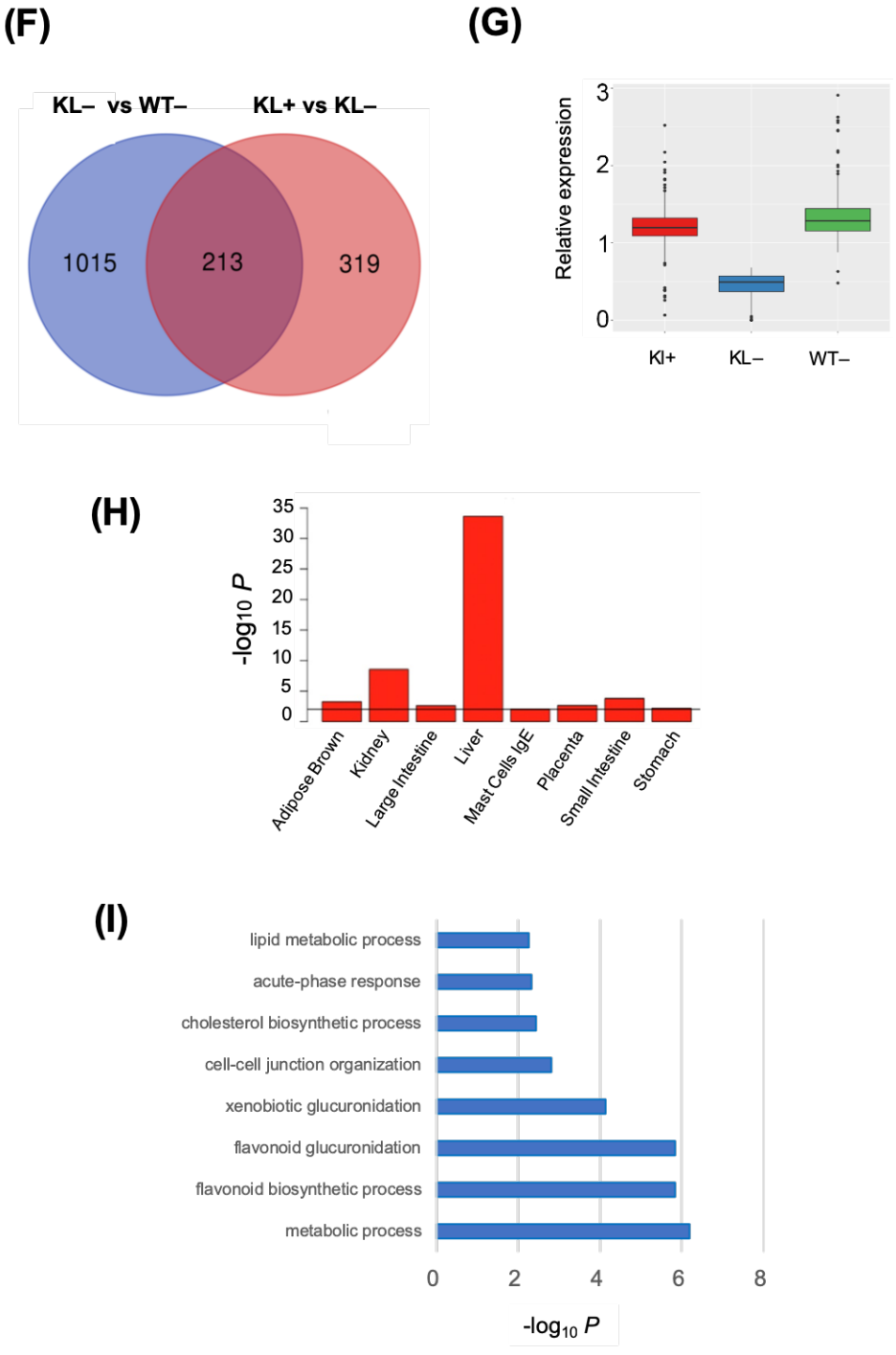

Figure 3. DEG analysis showed that liver function in klotho mice improved after administration of JTT

Number of up-regulated genes and down-regulated genes from the DEG data for the comparison (A) of KL– vs WT– and (B) of KL+ vs KL–. Cten analysis of (C) 1228 down-regulated genes in KL– in the comparison of KL– vs WT–, (D) 1352 up-regulated

genes in KL–in the comparison of KL– vs WT–, and (E) 532 up-regulated genes in KL+ in the comparison of KL+ vs KL–. (F) A Venn diagram of transcriptome comparisons from KL+ vs KL– and KL– vs WT–. Two hundred thirteen genes were shared between the comparisons. (G) Box plots of 213 gene expression data show a significant decrease in KL– in comparison with that in WT– and a significant increase in KL+ in comparison with KL–. Values along the vertical axis are normalized based on the overall average. (H) Cten analysis (http://www.influenza-x.org/~jshoemaker/cten/) for 213 genes that were differentially expressed in the comparison between KL+ vs KL– and between KL– vs WT–. The horizontal line indicates $P = 0.01$. (I) Bar graphs showing $-\log_{10} P$ of GO terms enriched for the 213 genes shown in (F). Only those terms with $P < 0.01$ are shown.

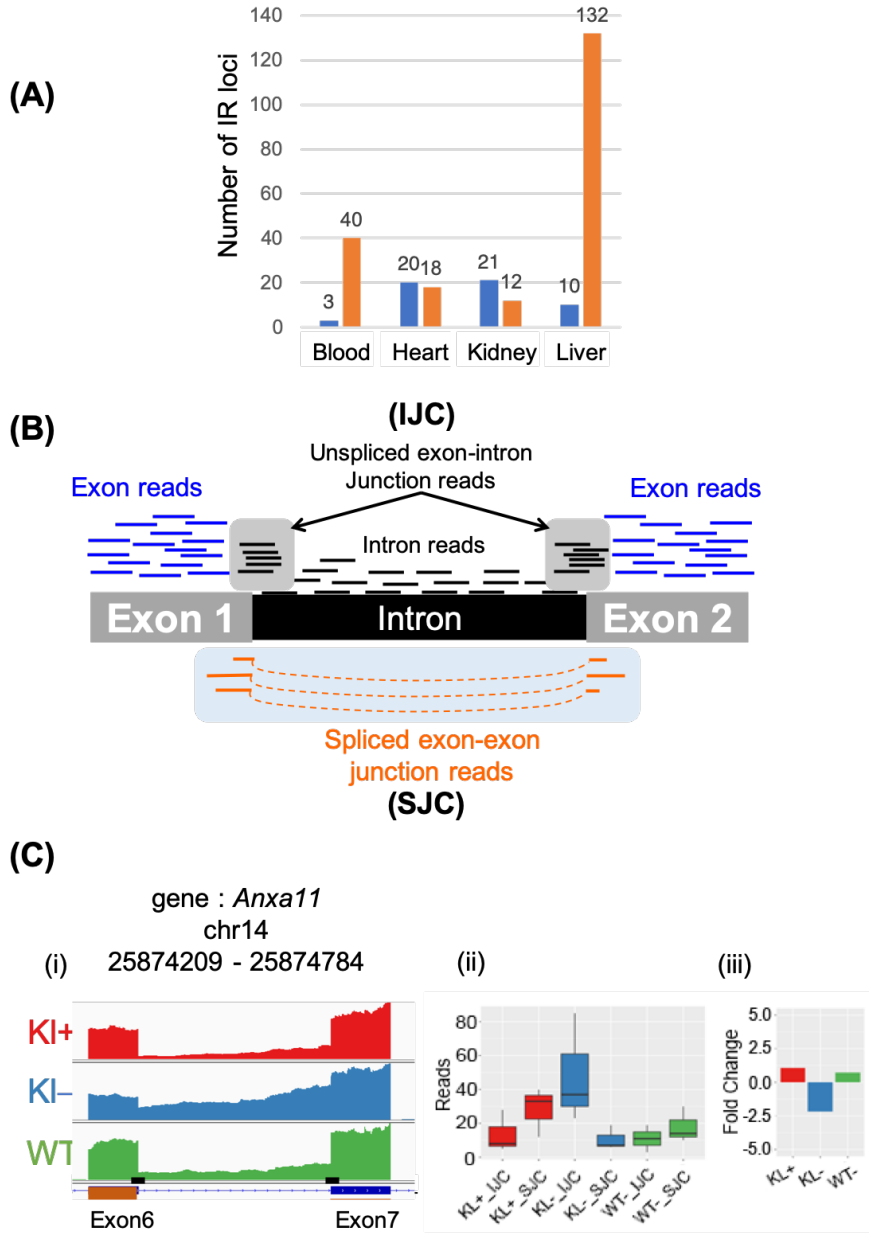

Figure 4. Quantification of IR events

(A) Among the four organs examined, liver had the most notable recovery of retained introns after administration of JTT. Bar graphs show the number of retained introns that decreased (in orange) or increased (in blue) in the four organs as a result of administration of JTT. Based on the rMATS analysis, genes with a significant change in IR in the comparison of KL+ vs KL– were divided into two groups. In the liver, the first group includes genes that showed a decrease in IR in KL+ (132 loci; DecIR type, implying that the fold change of KL+ was larger than that of KL–), and the second

1135 includes genes with an increase in IR in KL+ (10 loci; IncIR type, implying that the fold
1136 change of KL+ was smaller than that of KL–). (B) The quantification of IR events from
1137 mRNA-seq data using rMATS. The IJCs represent the reads containing the intron
1138 sequence at the junction. The SJCs represent the reads without intron sequences at the
1139 junction. (C) (i) The mapping results from KL+, KL–, and WT– are shown for a single
1140 gene, *Anxa11*, using Integrative Genomics Viewer (IGV). Thick black bars indicate the
1141 sites of junctions in the reads where SJCs and IJCs were analyzed. (ii) Read counts from
1142 KL+, KL–, and WT– for IJCs and SJCs. (iii) FC in the number of SJCs relative to IJCs
1143 for KL+, KL–, and WT–.
1144
1145
1146
1147

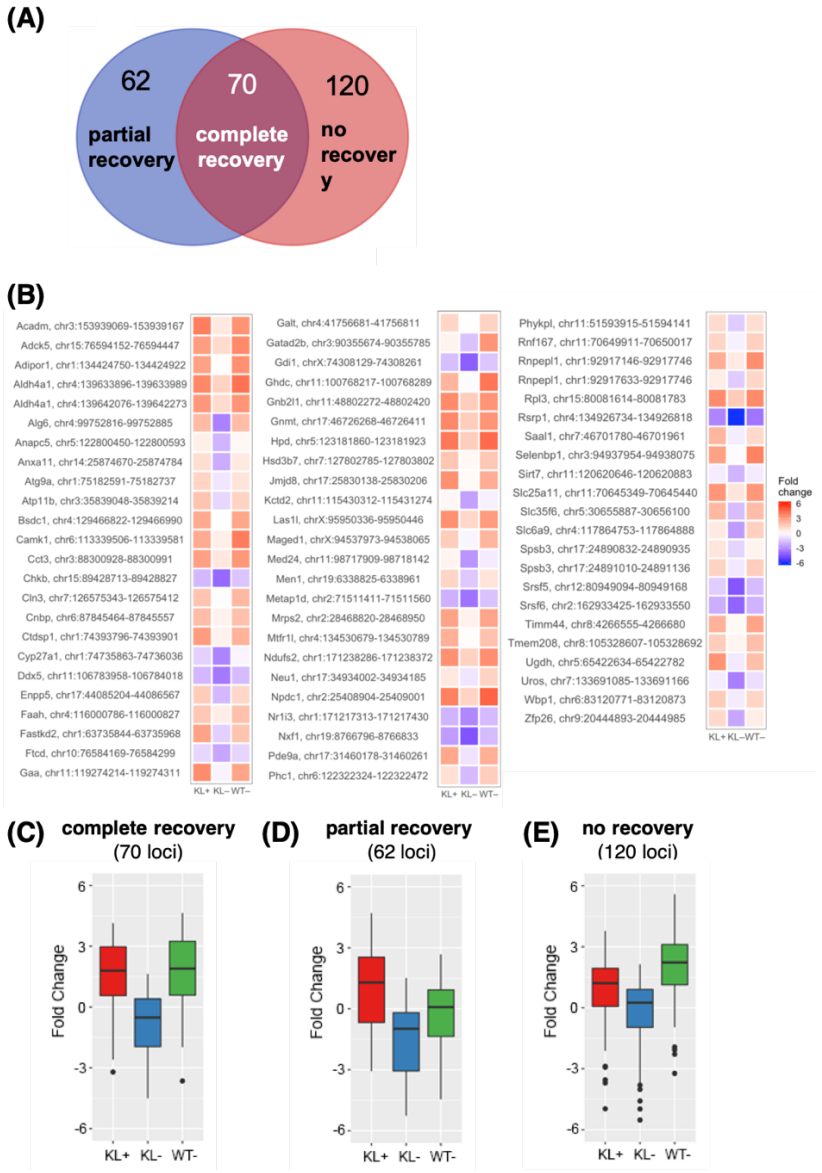

Figure 5. Seventy loci of complete recovery show a typical V-shaped pattern of recovery

(A) A Venn diagram of two types of loci, the DecIR type (blue circle) in the comparison of KL+ and KL– and the IncIR type (red circle) in the comparison of KL– and WT–. Three categories, namely “partial recovery”, “complete recovery”, and “no recovery” loci, are distinguishable. (B) Heat map illustration of FC values of loci in KL+, KL–, and WT– for the 70 “complete recovery” loci. (C–E) Boxplots of the FC values of (C) the 70 “complete recovery” loci, (D) the 62 “partial recovery” loci, and (E) the 120 “no-recovery” loci in KL+, KL–, and WT–.

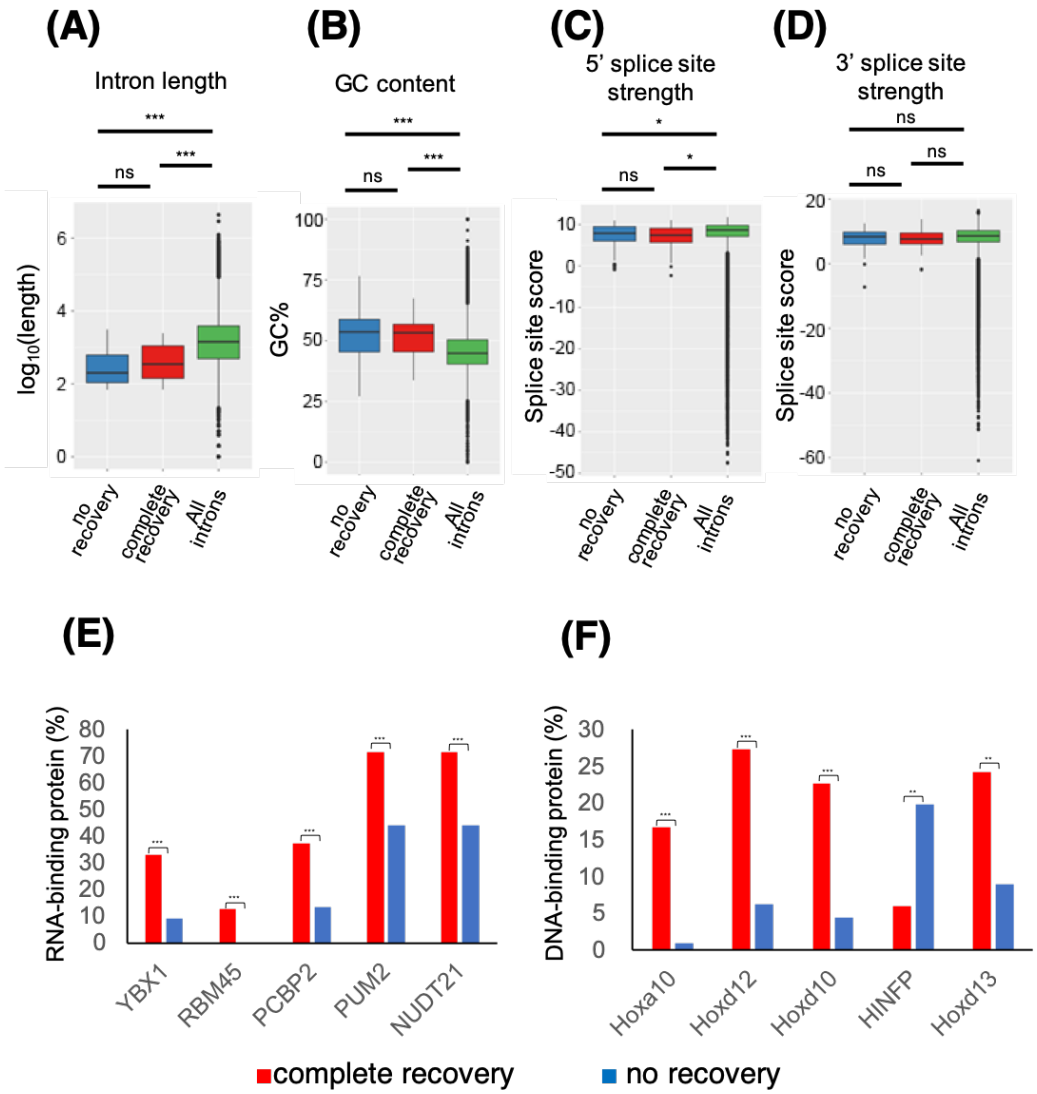

Figure 6. Retained intron loci have distinguishing characteristics

(A–D) Boxplots showing (A) intron lengths, (B) the GC percentage in intron sequences, and the strength score of the (C) 5' and (D) 3' splice sites compared among three groups of introns, namely "no recovery", "complete recovery", and all introns from liver-expressed genes (254,005 loci). *$P \leq 0.05$, ***$P \leq 0.001$, unpaired Student's *t*-test; ns, not significant. (E, F) Bar graphs showing percentage of loci in the "complete recovery" and "no recovery" groups that have (E) motifs for RNA-binding proteins within the intron or (F) motifs for DNA-binding proteins in the promoter region. **$P \leq 0.01$, ***$P \leq 0.001$, Fisher's test.

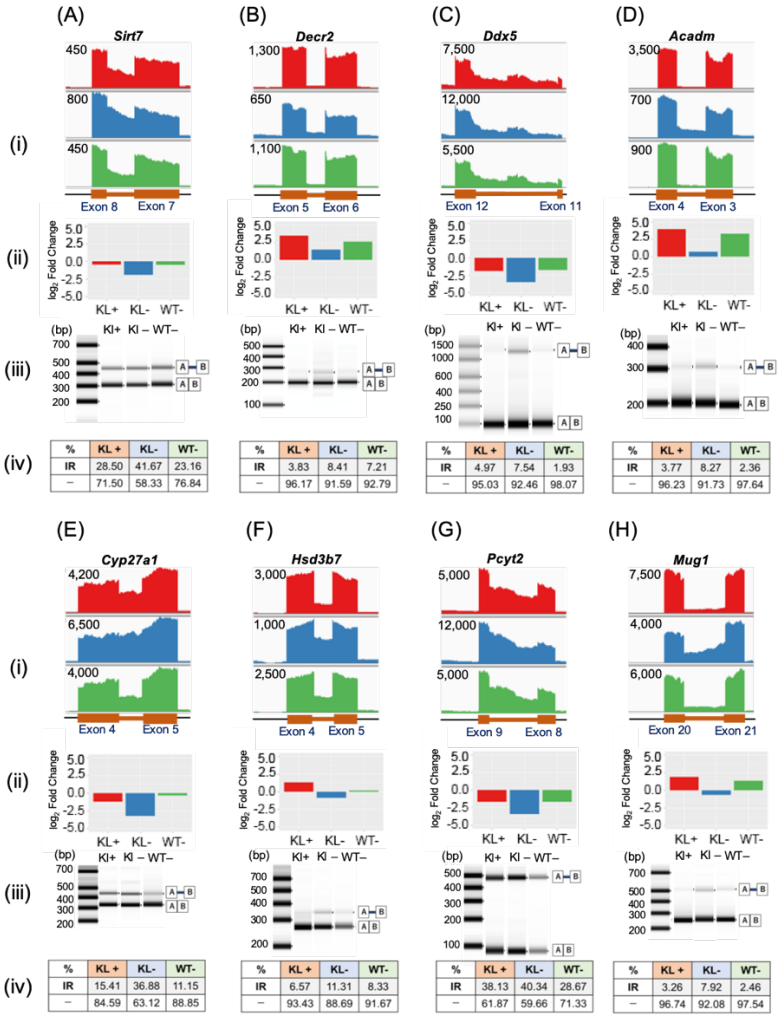

Figure 7. RT-PCR validation of retained introns and their recovery after administration of JTT

(A–H) Eight genes, (A) *Sirt7*, (B) *Decr2*, (C) *Ddx5*, (D) *Acadm*, (E) *Cyp27a1*, (F) *Hsd3b7*, (G) *Pcyt2*, and (H) *Mug1*, were subjected to the following analyses. (i) IGV mapping of reads from KL+, KL–, and WT–. The numbers shown to the left of each map represent read counts. (ii) Bar graphs showing fold changes in SJCs relative to IJCs for KL+, KL–, and WT–. (iii) RT-PCR validation of RNA expression from KL+, KL–, and WT–. A and B indicate exons, with the intervening intron indicated for the higher-molecular-weight product. (iv) The ratio of each transcript as determined using TapeStation. Data from KL+, KL–, and WT– are shown in red, blue, and green, respectively.

1187

(A)

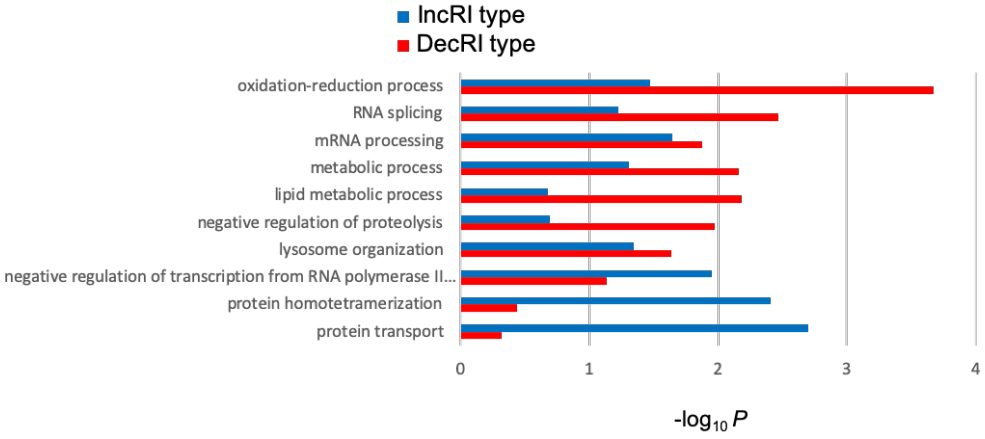

(B)

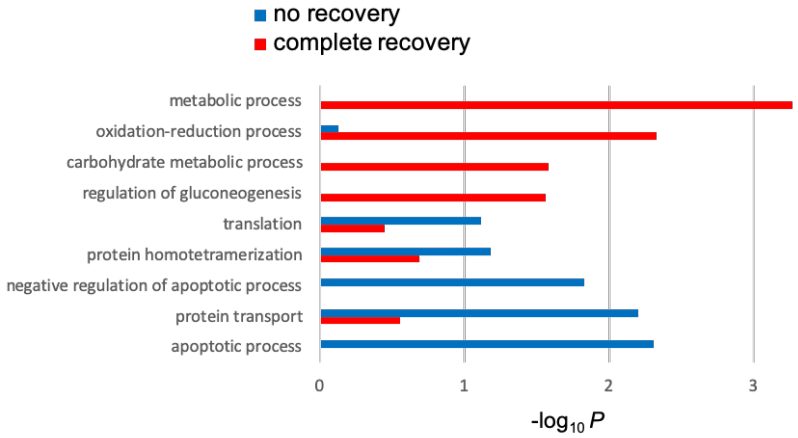

(C)

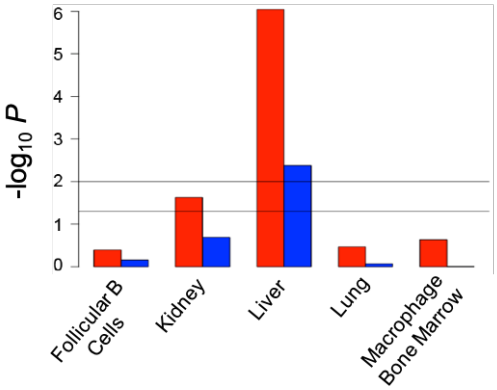

1188

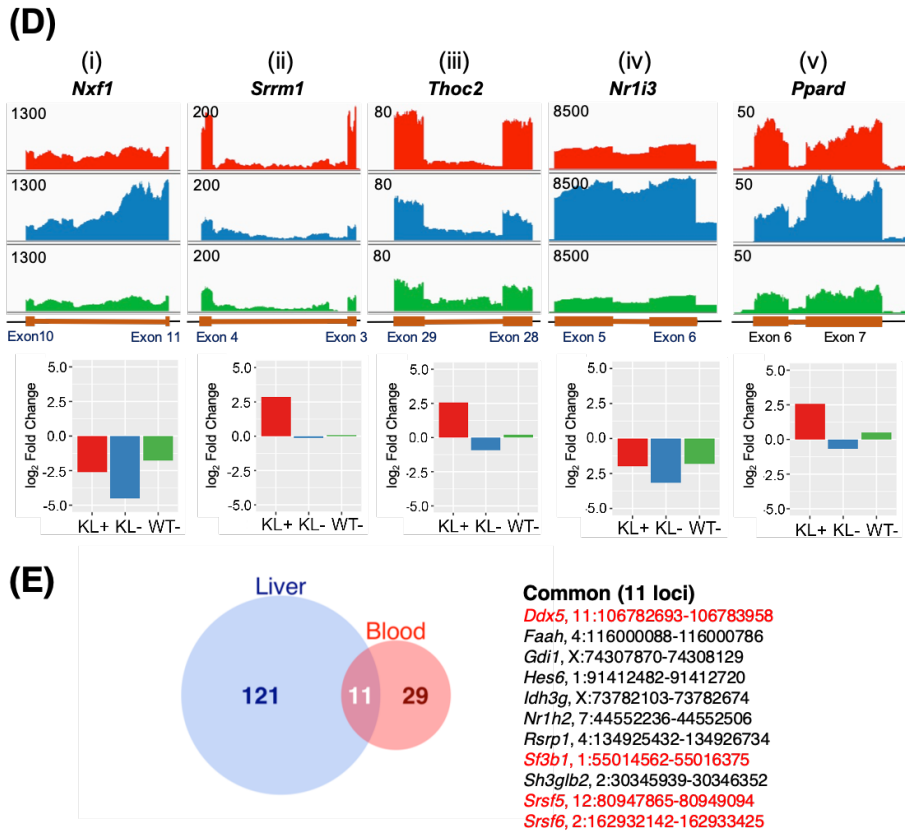

Figure 8. Genes with recovered retained introns in liver have the characteristics of liver-specific genes.

(A) Bar graphs showing $-\log_{10} P$ of GO terms enriched for genes whose IR events were significantly changed in the liver. Red bars show enrichment of GO terms in genes with the DecIR type in KL+ in the KL+ and KL– comparison, and blue bars show enrichment of GO terms in genes with the IncIR type in KL– in the KL– and WT– comparison. (B) Bar graphs showing $-\log_{10} P$ of GO terms enriched for genes defined as "complete recovery" (red bars) and "no recovery" (blue bars) loci. (C) Cten analysis for genes expressed in the liver with the DecIR type in red and those with the IncIR type in blue as shown in Fig. 5A. Horizontal lines indicate $P = 0.05$ (lower line) and 0.01 (upper line). (D) The mapping results from IGV for five gene loci, (i) *Nxf1*, (ii) *Srrm1*, (iii) *Thoc2*, (iv) *Nr1i3*, and (v) *Ppard*, are shown (upper). Bar graphs (lower) show the FC using the IJC and SJC values for KL+, KL–, and WT–. (E) Eleven genes were shared in common between the liver and blood in the recovery process of IR after administration of JTT. The Venn diagram (left) of the DecIR genes that were shared in the liver and the blood. The overlapping genes between blood and liver are listed (right), among which splicing-related genes are shown in red.

1208

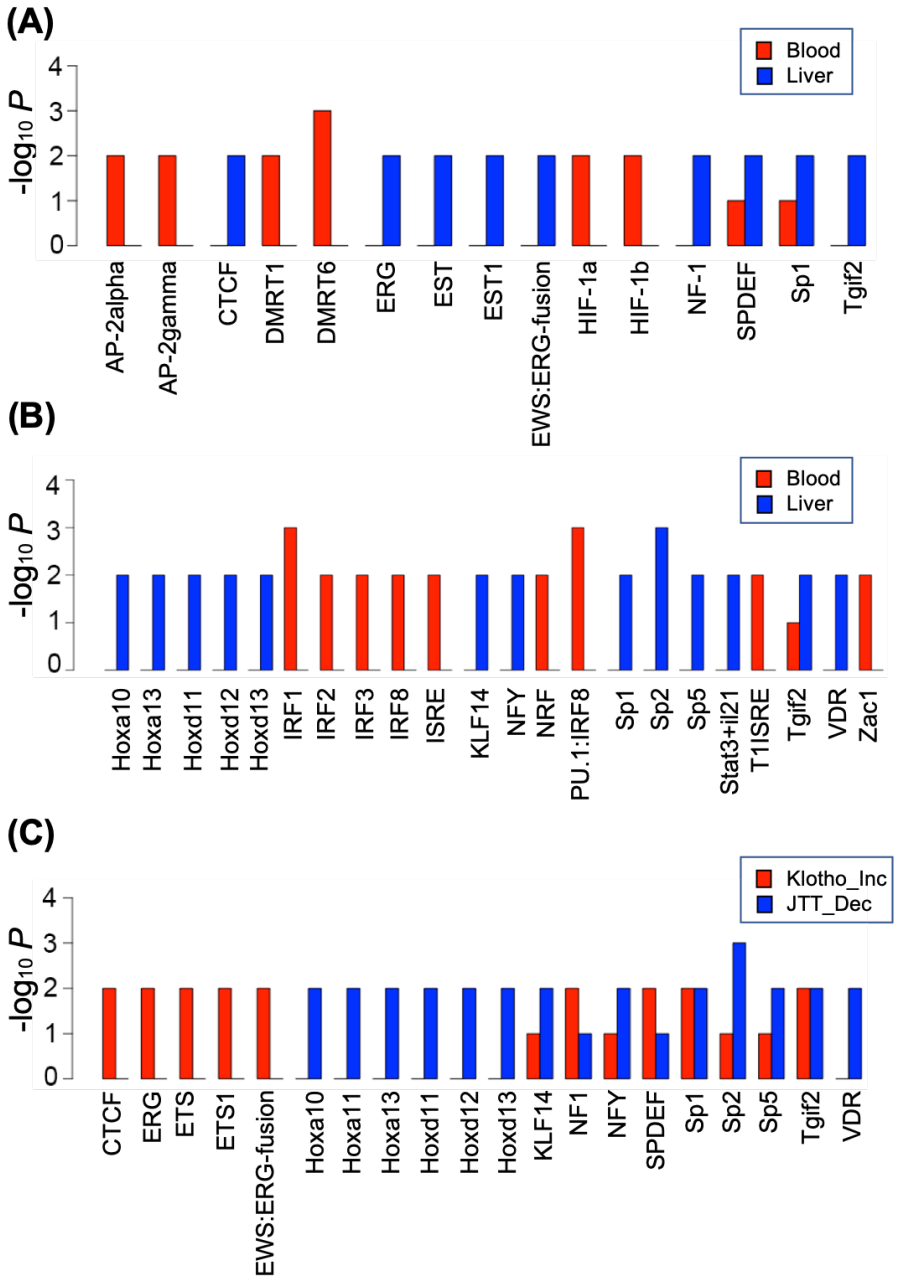

1209
1210
1211

(D)

(i)

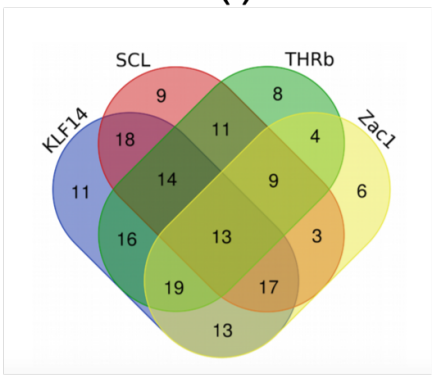

(ii)

TF	num of genes
KLF14(Zf)	121
Sp2(Zf)	120
Sp5(Zf)	104
KLF5(Zf)	102
SCL(bHLH)	94
THRb(NR)	92
Zac1(Zf)	84
KLF6(Zf)	83
ETV1(ETS)	82
AR-halfsite(NR)	81

(E)

(i)

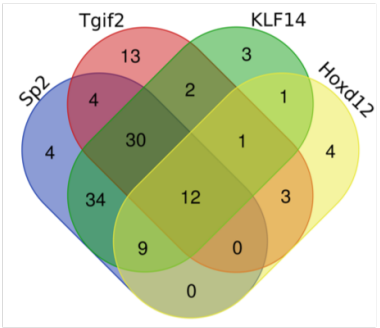

(ii)

TF	num of genes
Sp2(Zf)	93
KLF14(Zf)	92
Sp5(Zf)	79
Tgif2(Homeobox)	65
Sp1(Zf)	52
NFY(CCAAT)	45
Hoxd11(Homeobox)	43
Hoxa13(Homeobox)	42
Hoxa11(Homeobox)	40
Hoxd13(Homeobox)	31

Figure 9. A very few TFs may control genes with DecIR as well as those with IncIR
(A) Bar graphs showing $-\log_{10}P$ of enrichment of the TF-binding motif in genes with IncIR from blood and liver. (B) Bar graphs showing $-\log_{10}P$ of enrichment of the TF-binding motif in genes with DecIR from blood and liver. (C) Bar graphs showing $-\log_{10}P$ of enrichment of the TF-binding motif in genes with IncIR and DecIR from liver. (D) Genes with IncIR may be controlled by a very few TFs. (i) Venn diagrams of the IncIR genes that have TF-binding motifs in the liver and (ii) the top 10 motifs represented in these genes. (E) Genes with DecIR may be controlled by a very few TFs. (i) Venn diagrams of the DecIR genes that have TF-binding motifs in the liver and (ii) the top 10 motifs represented in these genes.

1226

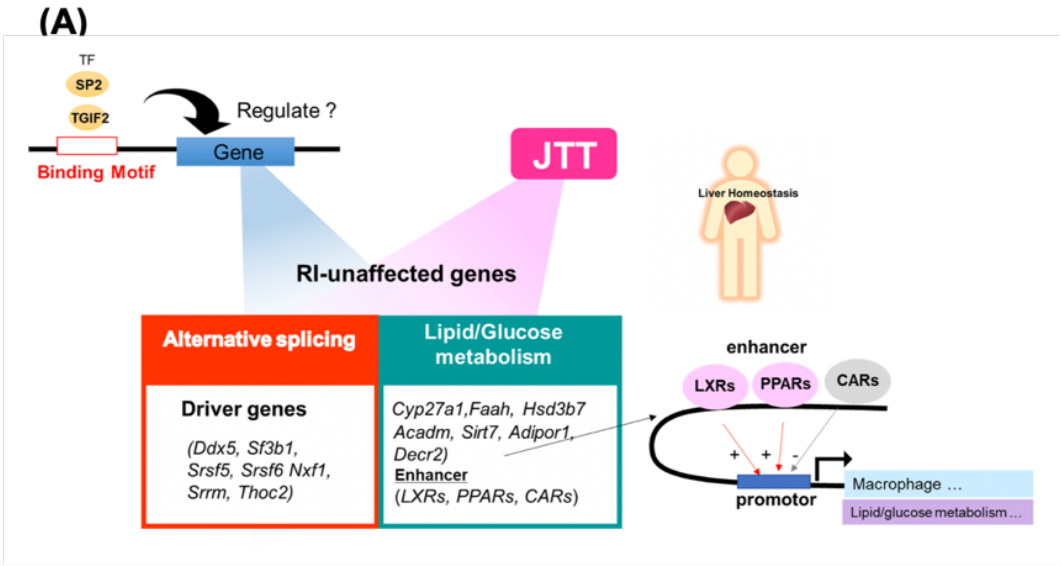

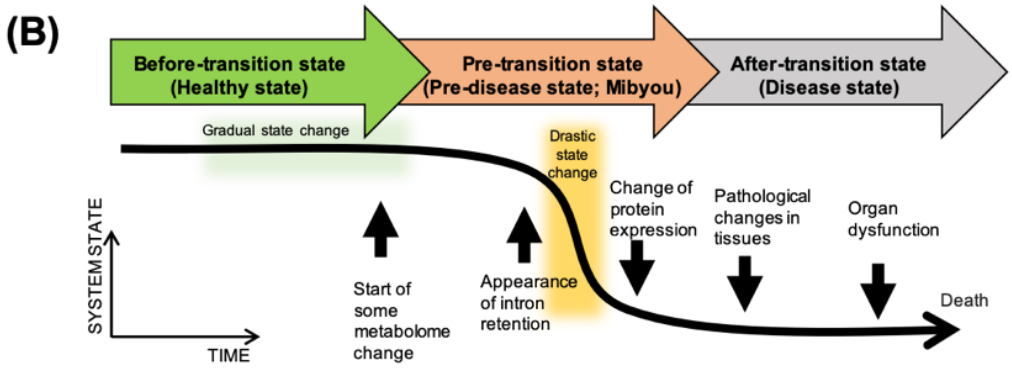

1227

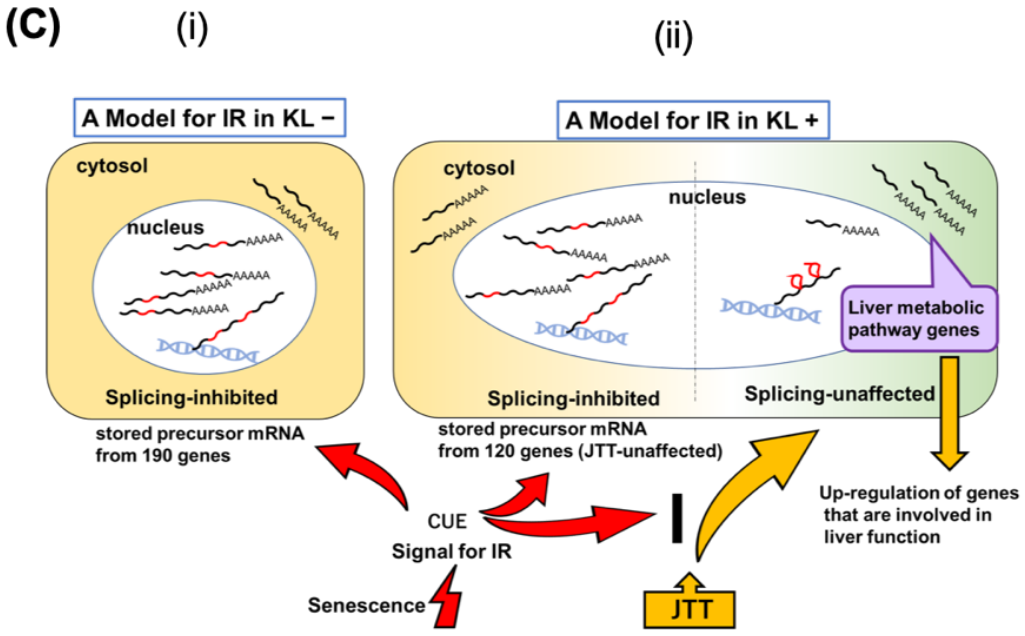

1228

Figure 10. IR is a marker of the pre-disease state and the recovery of retained introns suggests the recovery to the normal state.

(A) Illustration of the functional orchestration of IR-recovered genes under surveillance of homeostasis within the host. Two categories of genes that are involved are shown: alternative splicing and the biological function lipid/glucose metabolism. We hypothesize that the surveillance of homeostasis affects which genes undergo IR recovery after JTT administration during the earlier stage of aging (7 weeks of age) from the pre-disease state to the normal state (see the Discussion). Except for genes for alternative splicing and lipid/glucose metabolism, several genes involved in mitochondria function and the immune system including macrophage function were included among 124 IR-recovered genes (Fig. 5A; 132 loci). *Polrmt*, *Uros*, *Sh3glb2*, *Idh3*, *Cyp27a1*, and *Hsd3b7* are involved in mitochondrial function. JTT protects mitochondrial function (Park et al., 2018), and a JTT-related multi-herbal medicine prevents mitochondrial dysfunction, providing a possible treatment for the prevention of Parkinson disease (Ko et al., 2018). In addition, the anti-tumor effect of JTT may rely partly on activation of mitochondria (Zheng et al., 2014). *Gdi1*, *Sh3glb2*, *Faah*, and LXRβ are involved in the immune system including macrophage function and interferon activity. JTT has been widely used as a palliative to treat cancer patients (Okumi and Koyama, 2014) and also to treat patients with bacterial infections such as acute otitis media (Kitamura et al., 2015). JTT also contributes to the maintenance of antibody titer in elderly people after influenza vaccination (Saiki et al., 2013). A number of animal studies have demonstrated an adjuvant effect of JTT, especially with respect to activation of innate immune cells such as macrophages, dendritic cells, natural killer cells, and natural killer T cells (Ishikawa et al., 2017). Microarray analysis indicates that the target of JTT might be the transcription machinery regulating the steady-state level of the type 1 interferon-related genes (Munakata et al., 2012). Oral administration of JTT can elevate the phagocytic activity of macrophage-like cells in the various tissues (Saiki, 2000, Takeno et al., 2015). Similarly, the phytoestrogen flavonoids found in Glycyrrhizae radix, one of the components of JTT, can enhance phagocytosis in a murine macrophage cell line, as we described previously (Kaneko et al., 2017). JTT contains various types of flavonoids, some of which have been identified as selective agonists of LXR, according to molecular-docking analysis *in silico* (Fouache et al., 2019). LXRs, PPARs, and CARs are nuclear receptors and regulate genes related to lipid/glucose metabolism and macrophage function. (B) Schematic representation of the disease process from the healthy state through the pre-disease state. Possible changes that occur in the body are shown with arrows. (C) A model to explain why a specific

subset of genes with IR was recovered in KL+ by administration of JTT. (i) In the case of KL−, it is presumed that ~200 pre-mRNAs containing retained introns were stored in the nucleus because of the stress signal induced by aging so that the cells can save energy. (ii) In the case of KL+, as liver metabolic stress was recovered after JTT administration, the improved condition of the liver cells led to enhanced post-transcriptional splicing among pre-mRNAs with retained introns involved in metabolism.

Table 1-1. Number of alternative splicing loci between KL+ and KL–

	A3SS		A5SS		SE		IR		MXE		Total	
	$P < 0.01$	FDR <0.05	$P < 0.01$	FDR < 0.05	$P < 0.01$	FDR <0.05	$P < 0.01$	FDR <0.05	$P < 0.01$	FDR <0.05	$P < 0.01$	FDR <0.05
Blood	16	1	13	4	58	6	69	10	4	0	160	21
Kidney	17	2	13	5	96	18	33	9	3	1	162	35
Heart	16	0	3	3	90	2	38	5	7	1	154	11
Liver	63	16	35	9	121	46	142	80	7	2	368	153

FDR: false discovery rate

A5SS: alternative 5' splice site

A3SS: alternative 3' splice site

SE: skipped exon

IR: Intron retention

MXE: mutually exclusive exons

Table 1-2. Number of alternative splicing loci with significant difference in liver

	SE	A5SS	A3SS	MXE	IR	Total
KL+/KL-	121	35	63	7	142	368
KL+/WT+	222	37	59	6	90	414
KL+/WT-	199	31	43	7	59	339
KL-/WT+	294	67	121	16	382	880
KL-/WT-	205	36	77	9	212	539
WT+/WT-	90	23	25	5	56	199

Table 2. Increase or decrease in IR ratio of splicing-related genes in blood, heart, kidney and liver by administration of JTT

Gene Symbol	IR locus	Blood	Heart	Kidney	Liver
Cdk11b	4:155625654-155625726				↓
Cdk16	X:20696836-20696921	↓			
Cdk5	5:24422388-24422497				↓
Celf1	2:91013402-91016565	↓			
Ddx5	11:106782693-106783958	↓			↓
Hnrnpl	7:8818532-28818643		↑		
Nxf1	19:8765031-8766796				↓
Sf3b1	1:55014562-55016375	↓			↓
Srrm1	4:135344669-135346734				↓
Srsf5	12:80947865-80949094	↓		↓	↓
Srsf6	2:162932142-162933425	↓			↓
Thoc2	X:41822871-41823361				↓
U2af1l4	7:30564101-30564202			↑	